Effect of Charge on Protein Ion Structure: Lessons from Cation-to-Anion, Proton-Transfer Reactions

Short Title: Charge, Protein Structure, and CAPTR

Theresa A. Gozzo, Matthew F. Bush*

Contribution from:

Department of Chemistry

University of Washington

Box 351700

Seattle WA 98195-1700

*Address correspondence to: mattbush@uw.edu

Abstract

Collision cross section values, which can be determined using ion mobility experiments, are sensitive to the structures of protein ions and useful for applications to structural biology and biophysics. Protein ions with different charge states can exhibit very different collision cross section values, but a comprehensive understanding of this relationship remains elusive. Here, we review cation-to-anion, proton-transfer reactions (CAPTR), a method for generating a series of charge-reduced protein cations by reacting quadrupole-selected cations with even-electron monoanions. The resulting CAPTR products are analyzed using a combination of ion mobility, mass spectrometry, and collisional activation. We compare CAPTR to other charge-manipulation strategies and review the results of various CAPTR-based experiments, exploring their contribution to a deeper understanding of the relationship between protein ion structure and charge state.

Keywords

CAPTR, charge reduction, ion mobility, ion/ion reactions, native mass spectrometry, proteins

Abbreviations

Alcohol dehydrogenase	ADH
Bovine serum albumin	BSA
Cation-to-anion, proton-transfer reactions	CAPTR
Cation-to-anion, proton-transfer reactions precursor	*P*
Cation-to-anion, proton-transfer reactions product	*C*
Charge-reduction, electron-transfer dissociation	crETD
Collision-induced unfolding	CIU
Denaturing, disulfide-intact	DI
Denaturing, disulfide-intact, supercharging	DISC
Denaturing, disulfide-reducing	DR
Denaturing, disulfide-reducing, supercharging	DRSC
1,5-diazabicyclo[4,3,0]non-5-ene	DBU
Electron-capture dissociation	ECD
Electrospray ionization	ESI
Electron-transfer dissociation	ETD
Gas-phase basicity	GB
Ion mobility	IM
Mass spectrometry	MS
Native-like, disulfide-intact	NI
Native-like, disulfide-intact, supercharging	NISC
Perfluoro-1,3-dimethylcyclohexane	PDCH
Pyruvate kinase	PK

59 **Table of Contents**

60 Abstract 1

61 Keywords 1

62 Abbreviations 2

63 I. Introduction 5

64 A. ESI and Charge-State Distributions 5

65 B. IM-MS of Protein Ions 7

66 C. Charge-State Manipulation 9

67 1. Solution Additives 9

68 2. Ion/Neutral Chemistry 9

69 3. Ion/Ion Chemistry 10

70 4. Atmospheric-Pressure Analogues 13

71 D. Combining Charge-State Manipulation and IM-MS 14

72 II. CAPTR Implementation and Effects on Mass Spectral Analysis 14

73 A. Instrumentation 14

74 B. Charge-State Determination, Mass Assignment, and Resolution 16

75 III. Effects of CAPTR on the Structure of Protein Ions 18

76 A. CAPTR of Protein Ions from Denaturing Solutions 18

77 B. CAPTR of Protein Ions from Native-Like Solutions 21

78 C. Comparing Solution Conditions for Single Proteins 22

D. Effects of Charge Density on Ion Structure 25
IV. Probing Energy Landscapes 27
A. Pre-CAPTR Activation 27
B. Post-CAPTR Activation 29
V. Comparison to Results from Other Charge-Reduction Strategies 31
A. Effects of Charge on Small, Single-Domain Proteins 32
B. Effects of Charge on Proteins with Internal Disulfide Bonds 34
C. Effects of Charge on Native-Like Ions of Larger Proteins 36
VII. Energetics 38
VII. Conclusions 41
Acknowledgements 43
References 44
Biographies 57

I. Introduction

In cation-to-anion, proton-transfer reactions (CAPTR), gas-phase protein cations are quadrupole-selected and reacted with even-electron monoanions to generate a sequential series of charge-reduced cation products (Laszlo & Bush 2015). CAPTR products are then analyzed using ion mobility (IM) mass spectrometry (MS). The precursors and products of CAPTR can also be manipulated using other MS-based techniques, including collisional activation, prior to mass analysis (Laszlo et al. 2016). We first introduce the foundations and context for these experiments, including charging during electrospray ionization (ESI), IM of ESI-generated protein ions, and methods for manipulating the charge states of protein ions. We then describe various aspects of CAPTR experiments, review the results of our CAPTR-IM-MS studies, and discuss how those results contribute to a deeper understanding of the relationship between protein ion structure and charge state.

A. ESI and Charge-State Distributions

Inherent to the formation of ions is the acquisition of charge. For example, subjecting proteins in solution to positive-mode ESI generates cations with excess protons. The charge states of proteins in solution, and *in vivo*, depend on the pH of the solution or cellular environment, amino acid composition, protein structure, and interactions with other molecules. Notably, Figure 1A shows that charge states of proteins in solution are uncorrelated with mass (Allen et al. 2013). In contrast, the charge states of ESI-generated ions are strongly correlated with mass for well-folded proteins and uncorrelated with the corresponding charge states in solution (Allen et al. 2013). This leads us to consider the factors that influence observed gas-

117 phase charge-state distributions, and additionally, how that charging affects the structures of gas-
118 phase ions relative to their condensed-phase counterparts.

119 A detailed discussion of proposed ESI mechanisms is beyond the scope of this review,
120 but the ionization process is important to answering these questions. There is no singly agreed
121 upon mechanism to date, but molecular size appears to play a role (Hogan et al. 2009; Kaltashov
122 & Mohimen 2005). The charged-residue model is often invoked when discussing the multiple
123 charging of macromolecules (Iavarone & Williams 2003; Kebarle & Verkerk 2009); however,
124 the charged-residue model alone does not explain all observations (Allen et al. 2013; Konermann
125 et al. 2013). For example, it doesn't explain the polarity dependence of protein ion charge-state
126 distributions: lower average charge states are observed for anions from negative-mode ESI than
127 for cations from positive-mode ESI (Figure 1B-E), though anions and cations have been found to
128 be similar in size (Allen et al. 2013). These observations and others have been used as evidence
129 to support the combined charged-residue, field-emission model, in which the charge states of
130 many protein ions are limited by competitive emission of charge carriers during the final stages
131 of analyte desolvation (Hogan et al. 2009; Allen et al. 2013). Positive-mode ESI is most used for
132 the study of proteins, so protein cations are the primary focus of this review.

133 In addition to molecular size, the observed charge-state distributions of macromolecules
134 can depend on solution conditions prior to ESI (Bohrer et al. 2008; Gadzuk-Shea & Bush 2018;
135 Kafader et al. 2020). Native-like solution conditions seek to preserve noncovalent interactions
136 from the solution environment into the gas phase; these are typically aqueous solutions at neutral
137 pH with similar ionic strength to physiological conditions (Kafader et al. 2020). Native-like
138 conditions produce narrow charge-state distributions with lower average charge states. In
139 contrast, denaturing solution conditions often contain organic solvent and/or have acidic pH;

generating ions from denaturing conditions yields wider charge-state distributions and higher average charge states (Kafader et al. 2020). Other factors that can affect the observed charge-state distribution in ESI include current and voltage (Han & Chen 2022), the position of the ESI emitter relative to the atmospheric-pressure interface to the mass spectrometer (Benesch et al. 2009), and other IM-MS instrument parameters (Wang & Cole 1997; Bush et al. 2010).

B. IM-MS of Protein Ions

IM-MS is sensitive to the structures of gas-phase ions, and it is increasingly being applied to questions of structural biology (Barth & Schmidt 2020). MS is sensitive to the mass and charge of ions, whereas IM is sensitive to the size, shape, and charge of ions. In IM, ions are propelled forward by an applied electric field (E) and slowed down by collisions with a background gas. Ions' mobilities (K) are calculated from their drift times (t_d) through a cell of length, L:

$$K = \frac{L}{t_d E} \tag{1}$$

Within the low-field limit, the kinetic energy imparted by the drift field is negligible compared to the thermal kinetic energy, and the collision cross section, Ω, can be calculated using K and the Mason-Schamp equation (Mason & McDaniel 1988):

$$\Omega = \frac{3ez}{16N}\left(\frac{2\pi}{\mu k_B T}\right)^{1/2}\frac{1}{K} \tag{2}$$

where e is the elementary charge, z is the ion charge state, N is the drift gas number density, μ is the reduced mass of the ion-drift gas pair, k_B is the Boltzmann constant, and T is temperature of the drift gas.

Since generating gas-phase ions is central to making IM-MS measurements, it is important to consider how charge affects the structures of the analytes. As mentioned previously,

ESI of proteins in denaturing solutions yields ions with higher charge than those generated from native-like solutions. IM results show that more highly charged ions also exhibit larger Ω values (Clemmer et al. 1995; Bohrer et al. 2008; Wyttenbach & Bowers 2011; Kafader et al. 2020). IM-MS experiments probing the effect of ESI solution conditions consistently show a strong link between charge and Ω (Clemmer et al. 1995; Shelimov & Jarrold 1997; Valentine & Clemmer 1997; Valentine et al. 1997b; Wyttenbach & Bowers 2011; Bleiholder & Liu 2019). For instance, ubiquitin ions generated by ESI from denaturing conditions of 1:1 water: acetonitrile with 2% acetic acid resulted in charge states 6+ to 13+ (Valentine et al. 1997b), whereas 4+ to 6+ were observed under native-like conditions of aqueous 200 mM ammonium acetate at pH 7 (Salbo et al. 2012). Denatured ions exhibited larger Ω values than native-like ions, suggesting unfolding and elongation of the structures. Interestingly, the 6+ ions from denaturing conditions exhibited multimodal Ω distributions: as shown in Figure 2, some ions exhibited Ω values similar to native-like 6+ ions and close to values calculated using crystal structures, whereas other ions exhibited larger Ω values indicative of partial unfolding (Valentine et al. 1997b). Such studies provided foundational insights into the contributions of solution conditions and charge state to the structures of gas-phase ions. To investigate these relationships more extensively, a variety of charge-manipulation strategies have been pursued.

This review focuses on the effects of charge state on the structures of protein ions. Note that charge state also contributes the Ω of an ion, even without any changes in structure, because of long-range interactions between the ion and drift gas (Hogan et al. 2011; Laszlo et al. 2017b; Canzani et al. 2018). The magnitude of this effect increases with the polarizability of the drift gas. Most results described in this review are based on IM measurements performed in helium gas, which has a very low polarizability and minimizes this effect (Canzani et al. 2018).

C. Charge-State Manipulation

1. Solution Additives

Supercharging or charge-reducing agents can be added to solution to generate different charge-state distributions after ESI (Lomeli et al. 2010; Sterling et al. 2010; Bornschein et al. 2011; Allen et al. 2013; Pacholarz & Barran 2016; Gadzuk-Shea & Bush 2018; Townsend et al. 2019; Kaldmäe et al. 2019; Lyu et al. 2020; Yang et al. 2021; Iavarone & Williams 2003). Generating ions from denaturing or supercharging conditions are common approaches to produce broader charge-state distributions (Sterling et al. 2011; Kafader et al. 2020), but these strategies typically result in greater spectral congestion due to the presence of many different highly charged ions with smaller differences in m/z, which can make it more challenging to resolve bound species or interfering components. Increasing charge may not produce desirable conditions for maintaining native-like structure; Coulombic repulsion can preferentially favor extended structures relative to compact structures (Rolland et al. 2022), and supercharging agents are associated with protein unfolding (Sterling et al. 2010, 2011; Gadzuk-Shea & Bush 2018). Charge reduction is advantageous because it creates additional charge states and can potentially resolve more species at higher m/z. A drawback to using solution-phase additives is that they can make it more challenging to isolate contributions from solution conditions, ionization, and gas-phase charge state on the structures of the resulting ions. Additionally, the entire sample is exposed to the charge manipulation agent, whereas some gas-phase techniques discussed below may enable the isolation of subpopulations of ions prior to charge reduction.

2. Ion/Neutral Chemistry

Gas-phase reactions can decouple ionization and charge modulation, so contributions from changes in charge can be isolated from solution-phase interactions. Gas-phase charge reduction can be accomplished by ion/neutral or ion/ion reactions. Ion/neutral reactions frequently utilize proton transfer. For example, protein cations can be reacted with vapors of neutral basic reagents, and the extent of charge reduction depends on the number of ion/reagent collisions, the thermodynamics of the reaction, and other factors that affect the fraction of ion/reagent collisions that lead to products, *i.e.*, the reaction efficiency (Ikonomou & Kebarle 1992; McLuckey et al. 1991a; Ogorzalek Loo & Smith 1994; Valentine et al. 1997a). Even with strong "proton sponges," this charge reduction strategy is not universal and may compete with ion/neutral clustering (Ikonomou & Kebarle 1992; McLuckey et al. 1991a; McLuckey & Stephenson 1998; Ogorzalek Loo & Smith 1994; Valentine et al. 1997a). As charge state decreases, the reaction efficiency also decreases, which limits the extent of charge reduction (McLuckey et al. 1991a; McLuckey & Stephenson 1998; Stephenson & McLuckey 1996a). The low volatility of some reagents also causes persistence in vacuum systems and limits usable pressures (Herron et al. 1996; Ikonomou & Kebarle 1992; McLuckey et al. 1991a).

3. Ion/Ion Chemistry

Ion/ion reactions benefit from long-range Coulombic attraction, exothermicity at all charge states, and the ability to quickly modulate or purge anions (McLuckey & Stephenson 1998). Ion/ion reactions primarily proceed through electron or proton transfer, though ion exchange or adduction can also occur (McLuckey & Stephenson 1998; Pitteri & McLuckey 2005). For reactions of multiply charged cations and singly charged anions, proton transfer and

electron transfer compete. Proton transfer is more likely when even-electron anions are used (McLuckey & Stephenson 1998):

$$[M + xH]^{x+} + A^{-} \rightarrow [M + (x-1)H]^{(x-1)+} + AH \quad (3)$$

This reaction yields a charge-reduced cation that is also even electron; fragmentation of these products is rare (Gunawardena et al. 2005; Herron et al. 1995). Electron transfer is more likely when a radical anion is used (McLuckey & Stephenson 1998):

$$[M + xH]^{x+} + A^{\bullet -} \rightarrow [M + xH]^{\bullet (x-1)+} + A \quad (4)$$

This reaction yields a charge-reduced cation that is odd electron, *i.e.*, a radical cation. When electron transfer yields products that have the *m*/*z* of the expected charge-reduced product, it is also possible that radical-induced cleavages occurred, but that fragments remain bound through noncovalent interactions (Gunawardena et al. 2005; Jhingree et al. 2017; Riley et al. 2017). Therefore, Reactions 3 and 4 may yield charge-reduced products that have very different structures. Although beyond the scope of this review, ion/ion chemistry enables many other exciting reactions (McLuckey & Huang 2009), including the ability to invert the polarity of protein ions (He et al. 2005) and form crosslinks that are sensitive to the gas-phase structures of protein ions (Cheung See Kit & Webb 2022).

The advent of electron-capture dissociation, ECD (Zubarev et al. 1998), and electron-transfer dissociation, ETD (Syka et al. 2004), techniques helped motivate additional electron-based charge-transfer studies (Abzalimov & Kaltashov 2010; Geels et al. 2006; Pitteri et al. 2005; Xia et al. 2008). In ECD, low-energy electrons are captured, forming odd-electron species, which frequently undergo fragmentation at the backbone N-C_α bonds (Syrstad & Turecček 2005; Turecček et al. 2008; Tureček & Julian 2013). In ETD, instead of free electrons, anions are used to transfer electrons to cations; ETD has been found to produce similar fragments to ECD (Pitteri

et al. 2005; Syka et al. 2004). Charge-reduced products are also observed from both ECD and ETD (Pitteri et al. 2005; Syka et al. 2004; Zubarev et al. 1998), but ETD has been used more extensively to intentionally generate those products (Jhingree et al. 2017; Lermyte et al. 2015; Pitteri et al. 2005; Yang et al. 2021). Both charge-reduction ETD (crETD) and electron transfer with no dissociation, *i.e.*, ETnoD, are used to describe the use of ETD as a charge-reduction technique. For ease of discussion, we'll use crETD to refer to both implementations for the remainder of the review. Some reagents that have been used for crETD are fluoranthene, azobenzene, 1,3-dicyanobenzene, 1,4-dicyanobenzene, and p-nitrotoluene (Abzalimov & Kaltashov 2010; Jhingree et al. 2017; Lermyte et al. 2015; Liu & McLuckey 2012; Yang et al. 2021).

Perfluorocarbons have several properties that are beneficial for proton transfer (McLuckey & Stephenson 1998). Foundational studies using perfluoro-1,3-dimethylcyclohexane (PDCH) as an anion source were particularly useful for reactions with protein cations. Many of these experiments were performed on a modified 3D quadrupole ion trap (Stephenson & McLuckey 1997). An ESI source produced peptide and protein cations, and an atmospheric-sampling, glow-discharge interface produced anions from vapors of PDCH. The ion trap was floated at a negative voltage for the accumulation of cations, a precursor ion isolation step followed (McLuckey et al. 1991b), and then the trap offset was switched to a positive voltage for the subsequent injection of anions. A period of mutual storage followed during which the voltage was held at or near zero, and ions were permitted to react. Anions were often removed, and then cations were detected. High-*m*/*z* measurements were made using resonance ejection (Kaiser et al. 1989).

Using this setup, ions of insulin, ubiquitin, cytochrome *c*, myoglobin, albumin, transferrin, phosphorylase B, and more were reacted with PDCH anions (Stephenson & McLuckey 1996a, 1997). From these experiments, key aspects of these reactions were revealed. For one, anions derived from PDCH formed no adducts with peptide and protein cations, but, for other anions studied, adduction to high-mass cations was observed (Stephenson & McLuckey 1996a). Furthermore, no evidence of product cation fragmentation was observed, despite the net exothermicity of the reactions (McLuckey & Stephenson 1998). It was additionally found that PDCH-derived anions resist electron transfer, likely due to their high electron affinity and the instability of radical products (Gunawardena et al. 2005). Finally, favorable reaction kinetics were demonstrated under pseudo-first-order conditions; rates increase with the square of the charge state, and the reaction efficiency is constant for all charge states (McLuckey et al. 1998; Stephenson & McLuckey 1996a). This work also highlighted the utility of proton-transfer reactions for assigning the charge state and mass of protein analytes as well as for resolving interfering signals (McLuckey & Stephenson 1998; Pitteri & McLuckey 2005).

4. Atmospheric-Pressure Analogues

As mentioned previously, it is useful to perform reactions within the mass spectrometer, but charge reduction can be performed at the instrument interface, for example, by positioning a corona-discharge ionization source (Campuzano & Schnier 2013; Ebeling et al. 2000) or an α emitter (Scalf et al. 2000) adjacent to the ESI emitter induces charge reduction. The first reported implementation of gas-phase ion/ion reactions of multiply charged ions used a y-tube reactor at atmospheric pressure coupled with a quadrupole mass filter (Loo et al. 1991; Ogorzalek Loo et al. 1992). In these cases, the reactant ion species are not specifically identified because they are

299 formed by discharge or α particle reactions with air or bath gas at near-atmospheric pressure. The
300 chemistry of the reactions is less clear. Ion/neutral reactions have also been performed at
301 atmospheric pressure by exposure of generated ions to nebulized base (Bornschein et al. 2011).
302
303 **D. Combining Charge-State Manipulation and IM-MS**
304 IM-MS has been combined with the full catalogue of charge-manipulation strategies to
305 achieve a range of goals including increasing the information content of experiments and probing
306 the effects of charge on ion structure. For example, Clemmer and coworkers performed
307 groundwork in incorporating IM after ion/neutral proton-transfer reactions of protein ions,
308 investigating the effects of multiple different reagents (Shelimov et al. 1997; Valentine et al.
309 1997b,a). The first instrument integrating an IM separation of charge-reduced products following
310 ion/ion reactions was reported by Badman and coworkers; it included three ion sources, a 3D ion
311 trap where ion/ion chemistry was performed, an IM drift tube, and a quadrupole-time-of-flight
312 mass spectrometer (Zhao et al. 2009). The implementation of CAPTR with IM-MS is described
313 in the following section. Selected results from IM-MS studies using different charge-reduction
314 strategies will be discussed in the *Comparison to Other Charge Reduction Strategies* section.
315
316 **II. CAPTR Implementation and Effects on Mass Spectral Analysis**
317 **A. Instrumentation**
318 CAPTR experiments were performed on a Waters Synapt G2 HDMS modified with a
319 radio frequency-confining drift cell (Allen et al. 2016) and a glow-discharge ionization source to
320 generate monoanions for ion/ion chemistry (Williams et al. 2010), as shown in Figure 3A. In
321 collaboration with František Tureček, this instrument has also been used to characterize the

322 structures of peptide ions and their ETD products (Marek et al. 2013; Pepin et al. 2014; Marek et
323 al. 2015; Pepin et al. 2016b,a). A nanoESI source was used to generate protein cations from
324 borosilicate capillaries with inner diameters of 0.78 mm pulled to a 1-3 μm tip for all studies. By
325 inserting a platinum wire into the wide end of the capillary, electrical contact with the solution
326 was established. The atmospheric-pressure interface was held at an elevated temperature of 120
327 °C for the duration of experiments to prevent fouling of the ion optics; some experiments used a
328 temperature-controlled source for independent control of the temperatures of the sample
329 capillary and MS interface since heat transfer to the capillary had been observed (Laszlo et al.
330 2017a). PDCH was placed in the solvent reservoir at room temperature, and nitrogen gas seeded
331 with the headspace vapor was introduced to a stainless-steel discharge needle positioned after the
332 sampling cone. $[PDCH–F]^-$ monoanions were generated by glow discharge, quadrupole selected
333 at *m*/*z* 381, and accumulated in the stacked-ring ion trap cell for 100 ms. The instrument was
334 then switched to positive polarity, and cations, the whole population or a quadrupole-selected
335 population, were transmitted through the cloud of anions for 1 to 10 s. During transmission, the
336 traveling-wave amplitude in the trap remained at 0 V for maximum spatial overlap of cations and
337 anions. Figure 3B shows the relative potentials applied to ion optics during anion fill and cation
338 transmission under minimal-activation conditions. Figure 3C shows the relative potentials during
339 experiments that activate cations before or after CAPTR. Residual precursor ions and charge-
340 reduced products were sent on to the drift cell, the collision cell, and then to the time-of-flight
341 analyzer. Unless otherwise stated, the drift gas was helium for the discussed experiments. The
342 use of this platform for characterizing the relationship between charge and gas-phase ion
343 structure is discussed in the *Effects of CAPTR on the Structures of Protein Ions* section.

The instrument geometry used for CAPTR is most similar to that of Badman and coworkers (Zhao et al. 2009). Our implementation differs from previous approaches in that ion/ion chemistry is performed in a stacked-ring ion guide, and the anion population is depleted significantly during most experiments, so pseudo-first order conditions are not maintained (Laszlo & Bush 2015). In previous approaches, the reaction time was tuned to preferentially form a specific charge-reduced product of interest, but with CAPTR a wider range of z values for charge-reduced products are observed simultaneously (Laszlo & Bush 2015).

B. Charge-State Determination, Mass Assignment, and Resolution

Although this review is focused on the effects of charge on protein ion structure, we also want to comment on the utility of CAPTR to aid in the interpretation of native mass spectra, which often exhibit congestion and narrow charge-state distributions that challenge charge-state assignments and determination of mass (McKay et al. 2006). Creating additional charge states helps alleviate the uncertainty in this process. Figure 4 shows a native mass spectrum of pyruvate kinase and the CAPTR mass spectrum of the isolated m/z 7200 ions (Laszlo & Bush 2015). Simulated mass spectra corresponding to charge state assignments of 31+, 32+, and 33+ for the precursor ion are plotted over the experimental spectra. Each of the simulated native mass spectra provides a reasonable representation of the experimental native mass spectrum, but only the simulated CAPTR mass spectrum for the charge-state assignment of 32+ agrees well with the experimental CAPTR spectrum. With CAPTR, the ambiguity in charge state was virtually eliminated. Adjacent mass spectral peaks that differ by one charge have increased spacing at higher m/z, so, for example, a 12+ ion of neutral mass 223.1 kDa, a 13+ ion of neutral mass 230.1 kDa, and a 14+ ion of neutral mass 237.3 kDa can be resolved in m/z space. Additionally,

increasing the number of mass spectral peaks provides more observations for mass determination. This is a benefit of any strategy that increases the available charge-state observations, but CAPTR both increases the number of observations and the spacing between peaks. The accuracy of the mass analyzer and the mass heterogeneity of the analytes stemming from incomplete desolvation, nonspecific adduction, covalent modifications, *etc.*, become the main contributing factors to mass uncertainty.

CAPTR can also increase the resolution of interfering species in congested mass spectra, analogous to previous approaches by McLuckey and coworkers in ion traps (McLuckey et al. 1998; McLuckey & Goeringer 1995; Stephenson & McLuckey 1996a,b). Improved resolution was demonstrated using yeast enolase and bovine serum albumin (Laszlo & Bush 2015). In the native mass spectra, peak overlap was observed, but after isolating an overlapped peak and performing CAPTR, the products were well resolved. After 12 CAPTR events, the mass spectral resolution was 54 compared to 0.016 for the precursors. The change in resolution with charge reduction depends on the effect of each CAPTR event on the peak width and centroid values of product ion distributions. The following equation predicts the resolution of two peaks as a function of the number of CAPTR events (n):

$$R_{CAPTR}(n) = \frac{\frac{m_x}{(z_x^*-n)} - \frac{m_y}{(z_y^*-n)}}{2\left[\sigma_x^*\left(\frac{z_x^*}{z_x^*-n}\right)+\sigma_y^*\left(\frac{z_y^*}{z_y^*-n}\right)\right]} \quad (5)$$

where m, z, and σ are mass, charge, and standard deviation of species x and y. z^* and σ^* signify the charge state and standard deviations of the initial precursor ion specifically. The relationship between charge and peak width is based on fundamental time-of-flight equations (Guilhaus 1995); this equation assumes that centroid values shift only because of the changes in charge

state. In sum, CAPTR provides a facile way to resolve components in high-mass, heterogeneous samples.

III. Effects of CAPTR on the Structure of Protein Ions

Observations of CAPTR with PDCH-derived monoanions support previous findings that proton transfer is the predominant charge-transfer pathway, rather than anion adduction or electron transfer (Laszlo & Bush 2015). Unlike electron transfer, no evidence for fragmentation has been observed during CAPTR experiments (Gadzuk-Shea & Bush 2018; Laszlo & Bush 2015, 2017; Laszlo et al. 2016, 2017a,b) These properties of CAPTR, in addition to the wide range of charge states produced for structural characterization and mass assignment, support its utility as an analytical platform. In this section, we review the results of CAPTR-IM-MS of various protein cations generated from different solutions.

A. CAPTR of Protein Ions from Denaturing Solutions

As discussed previously, ions generated from denaturing solutions yield more highly charged ions with larger Ω values, indicating varying degrees of protein unfolding. By monitoring changes in Ω, we used CAPTR to investigate whether charge reduction can mitigate some of the structural effects associated with denaturing conditions. Studies also helped investigate the relationship between protein mass, Ω, and the extent of refolding with charge reduction. Ions of ubiquitin (8.6 kDa, monomer), cytochrome *c* (12 kDa, monomer), lysozyme (14.3 kDa, monomer), bovine serum albumin (BSA, 66 kDa, monomer), and antibodies, IgG1 (149 kDa, heterotetramer) and IgG4 (156 kDa, heterotetramer), were probed using various denaturing conditions. Ubiquitin and cytochrome *c* ions were both generated from 70:30

411 water:methanol acidified with trifluoroacetic acid to a pH of 2 (Laszlo et al. 2016, 2017a). 5+ to
412 13+ ubiquitin ions were observed from ESI, and from each precursor ion, CAPTR produced ions
413 as low as 3+ in charge (Laszlo et al. 2016). For ease of discussion CAPTR ions will be
414 represented by "*P*→*C*" for the remainder of the review where "*P*" is the precursor ion charge
415 state and "*C*" is the product ion charge state. For example, ubiquitin 13→3 specifies the 3+
416 CAPTR product ion generated from the 13+ precursor.
417 Figure 5A shows the Ω distributions for the 13→*C* ubiquitin ions. With increasing
418 numbers of CAPTR events (*i.e.*, decreasing *C*), the distributions shift to smaller Ω values. The
419 distributions appear relatively symmetric for large and small values of *C*, whereas the
420 distributions appear multimodal for intermediate values of *C*. The largest compaction for
421 denatured ubiquitin was observed for the 13→3 ions; this corresponds to a 50% decrease in Ω,
422 indicating significant refolding upon reduction in charge by 10 CAPTR events (Laszlo et al.
423 2016). Figure 5B shows the Ω values found for all *P*→*C* ubiquitin ions — these values depend
424 strongly on *C* and weakly on *P*. Differences between selected *P*→*C* ubiquitin ions will be
425 discussed in the *Pre-CAPTR Activation* and *Post-CAPTR Activation* sections.
426 Generated from the same solution conditions, cytochrome *c* cations as high as 18+ in
427 charge were observed (Laszlo et al. 2017a). Figure 6A shows the Ω distributions for the 18→*C*
428 cytochrome *c* ions; these distributions follow the general trends with decreasing *C* that were
429 described for the 13→*C* ubiquitin ions. The 18+ precursor ions exhibited a near 56% decrease in
430 Ω on charge reduction to 4+ and 3+, corresponding to 14 or 15 CAPTR events. To compare with
431 ubiquitin after 10 CAPTR events, cytochrome *c* 18→8 compacted by 30%. Interestingly,
432 cytochrome *c* 13→3 ions, also produced by 10 CAPTR events, compacted by 49%. Lysozyme
433 ions were generated by ESI from 1:1 water:acetonitrile with 0.2% acetic acid (Laszlo et al.

2017b). Under these conditions, 8+ to 13+ ions were produced. The 13→3 ions were the lowest-*z* CAPTR products observed with a corresponding 37% decrease in Ω. BSA ions, which are much larger in mass than lysozyme ions, were generated from 70:30 water:methanol with 0.2% formic acid (Gadzuk-Shea & Bush 2018). Ions up to 45+ in charge were subjected to CAPTR. Following 35 CAPTR events, the 45→10 ions decreased 48% in Ω from that of the precursor (Figure 7C). After 10 CAPTR events, Ω decreased by only 10%. IgG1 and IgG4 ions were generated by ESI from aqueous 0.1% acetic acid; these ions are over twice as large in mass as BSA ions (Gozzo & Bush, manuscript in preparation). 49+ ions were the ions of highest *z* subjected to CAPTR, yielding products as low in *z* as 15+ and 16+ for IgG1 and IgG4, respectively (33 to 34 CAPTR events). The parallel decrease in Ω was 21% for IgG1 and 17% for IgG4. After 10 CAPTR events, 49→39 ions had only decreased by 5.4% and 4.3% in Ω for IgG1 and IgG4, respectively.

A summary of the results for CAPTR of denatured protein ions can be viewed in Figure 8A and 8C. Across the board, protein cations generated from denaturing solutions all refolded to some extent following CAPTR. The extent to which, if at all, removing excess charges may enable protein ions to form new interactions that are also present in the corresponding native structures is unclear. For example, molecular dynamics simulations of 13+ ubiquitin in the gas phase following sequential proton stripping results in the formation of increasingly compact structures that yield calculated Ω values that are qualitatively similar to many of our experimental observations for the CAPTR products of 13+ ubiquitin generated from a denaturing solution (Sever & Konermann 2020). The proton-stripped 3+ ions from the simulations had calculated Ω values similar to those measured for native-like ubiquitin ions (Wyttenbach & Bowers 2011; Salbo et al. 2012) and similar to those previously calculated for native structures

of ubiquitin (Bleiholder et al. 2015; Jurneczko & Barran 2011). However, the molecular-dynamics structures were "inside-out", with new electrostatic interactions on the interior and hydrophobic residues on the exterior, as shown in Figure 9 (Sever & Konermann 2020). Additional simulations would benefit our understanding of the specific structural changes that occur at the molecular level following individual CAPTR events, especially for ions that exhibit Ω distributions that depend strongly on how they were formed (*e.g.*, 7+ ions from different solution conditions or from different numbers of CAPTR events). A trend between the degree of compaction and mass was also observed. As the ions increased in mass, the level of collapse in Ω from precursor ions to CAPTR products tended to decrease. This trend will be discussed further in the *Effects of Charge Density on Ion Structure* section.

B. CAPTR of Protein Ions from Native-Like Solutions

CAPTR was also applied to investigate the relationship between Ω and charge for protein ions generated from native-like conditions. Native-like solution conditions were the same for all protein cations probed: aqueous 200 mM ammonium acetate at pH 7. Cytochrome *c*, lysozyme, BSA, and IgG proteins were probed under both denaturing and native-like conditions, so they will be discussed first. The observed charge states were lower overall when compared to denaturing conditions, as expected. The most-intense charge states observed directly from electrospray were 6+ to 8+ for both cytochrome *c* and lysozyme. The 7+ cytochrome *c* precursor ions gave rise to CAPTR products as low as 3+ in *z*, corresponding to 4 CAPTR events (Laszlo et al. 2017a). The 7→3 ions were observed to be 11% smaller than their 7+ precursors (Figure 6B). Lysozyme 8+ precursor ions yielded lowest-*z* CAPTR products of 3+ as well; these were

8.4% smaller than their precursors (Laszlo et al. 2017b). For comparison, lysozyme 7→3 products were only about 6.3% smaller than the 7+ precursors.

CAPTR of the native-like ions of BSA yielded a maximum compaction of 6% for the 17→6 ions, corresponding to 11 CAPTR events (Gadzuk-Shea & Bush 2018) as shown in Figure 7D. From recent work probing IgG1 and IgG4 ions, maximum relative decreases in Ω of 2.3% and 2.2% were observed for the IgG1 25→13 ions and IgG4 26→14 ions, respectively (Gozzo & Bush, manuscript in preparation). 12 CAPTR events occurred in both cases. Additional native-like proteins probed by CAPTR included avidin (64 kDa, homotetramer), streptavidin (53 kDa, homotetramer), and alcohol dehydrogenase (147 kDa, homotetramer). Relative to their precursor ions, the maximum decreases in Ω values of the product ions were 2.9%, 2.3%, and 3.6% for avidin, streptavidin, and alcohol dehydrogenase, respectively, which occurred within the first few CAPTR events (Figure 10).

A summary of the results for CAPTR of native-like protein ions is shown in Figure 8B and 8D. Overall, minimal compaction was observed with charge reduction by CAPTR indicating that the excess charges on native-like ions have a relatively small impact on Ω. Less charge-state dependence was observed than for the unfolded ions generated from denaturing solutions. Ω values of cytochrome *c* and lysozyme exhibited a stronger dependence on *C* than those of the other proteins studied. Trends in this data and comparisons to those for denatured ions will be discussed in the *Effects of Charge Density on Ion Structure* section.

C. Comparing Solution Conditions for Single Proteins

In addition to examining the effect of charge state on protein ions spanning a range of masses and Ω values, CAPTR-IM-MS was used to investigate the relationship between Ω and

charge reduction for gas-phase ion structures of a single protein generated from different solution conditions. Our broadest study of the relationship between solution conditions, charge state, and Ω was one in which bovine serum albumin, BSA, ions were generated from five different solutions ranging from native-like to very disruptive (Gadzuk-Shea & Bush 2018). These conditions are referred to as native-like, disulfide-intact (NI); native-like, disulfide-intact, supercharging (NISC); denaturing, disulfide-intact (DI); denaturing, disulfide-intact, supercharging, (DISC); and denaturing, disulfide-reducing, supercharging (DRSC), as described in the original work (Gadzuk-Shea & Bush 2018). The more disruptive the original solution, the higher the charge states, the wider the charge-state distributions, and the larger the initial Ω values. Despite some overlap in the observed charge states produced (DISC and DRSC), none of the observed Ω values overlapped, indicating that ion structure depended strongly on the original solution conditions.

A subset of BSA ions from each condition was selected and subjected to CAPTR (Figure 7). Ω values of $P \rightarrow C$ ions from both DRSC (P = 70 and 80) and DISC (P = 50, 60, 70, and 80) conditions depended weakly on P and decreased monotonically with decreasing C. Ions from DI conditions exhibited lower charge states than those from DISC conditions, so the selected precursor was 45+. A steady decrease in Ω was observed for most $45 \rightarrow C$ ions, except for 35+ to 40+ products, which all had similar Ω values. Compared to ions from native-like conditions, ions from denaturing conditions exhibited more significant compaction with decreasing C due to refolding. From NISC conditions, precursors of charge 18+ to 21+ were selected. For P = 19 to 21, a steeper decrease in Ω was observed for the first CAPTR event with smaller decreases in Ω for the remaining charge reduction down to C = 6. $18 \rightarrow C$ ions from NISC conditions were all similar in Ω. Some ions from NISC conditions exhibited weak dependence on P, *e.g.*, the $P \rightarrow 14$

ions increase in Ω with increasing *P*, but the lowest *C* ions (6+) exhibited no trend in Ω with *P*. From NI conditions, *P* = 15 to 17, and Ω values for the *P*→*C* ions were all similar to each other, suggesting no significant dependence on the charge state of the precursor or product.

When comparing ions across conditions, *P*→*C* ions from denaturing conditions were all larger than the corresponding *P*→*C* ions from NISC conditions, which were all larger than those from NI conditions. *P*→*C* ions of the same *C* from DISC and DI conditions were similar in Ω. Ions from DRSC conditions were larger for high *C*, but the difference decreased with decreasing *C*. The rate of compaction with each CAPTR event was similar for ions from both DISC and DRSC conditions for $C \geq 36$, but both rates of compaction increased for $C < 36$. The DRSC compaction rate increased more, leading to the convergence of Ω values at low *C*. The difference between these two conditions was the presence or absence of disulfide bonds. Ions from DRSC conditions were more able to extend to larger structures than ions from DISC or DI conditions and were also able to refold more with each CAPTR event, emphasizing the constraining nature of disulfide bonding on the structures of these ions.

Another notable observation was that *P*→*C* ions from denaturing conditions with *C* values also observed from native-like conditions did not compact down to similar Ω values to the *P*→*C* ions from NI conditions — they remained about 30% larger. This result suggests that these ions retained some aspects of their solution-phase structures, even as they folded to smaller Ω with each CAPTR event. Finally, even though ions from NISC conditions decreased in Ω with decreasing charge state, they remained larger than ions from NI conditions for all charge states, indicating that protein structure is perturbed with supercharging by sulfolane. These structural changes were not mitigated by CAPTR, *i.e.*, supercharging can cause irreversible changes to the structures of protein ions.

548 In summary, these results suggest that gas-phase ions retain some aspects of their
549 solution-phase structure in the gas phase. CAPTR revealed that the Ω values of product ions can
550 depend simultaneously on the original solution conditions, *P*, and *C*. These experiments suggest
551 that protein ions have a memory of their prior structures from solution, and their gas-phase
552 structures respond to charge reduction and collisional activation accordingly.
553
554 **D. Effects of Charge Density on Ion Structure**
555 Together, the results discussed above suggest that charge density, as represented by *m*/*z*,
556 is a significant factor governing the overall impact of charge on gas-phase ion structures.
557 CAPTR-IM-MS experiments showed that, without exception, the Ω values of protein cations
558 generated from denaturing solution conditions had a stronger dependence on charge than protein
559 cations generated from native-like conditions. Denatured ions experienced significant refolding
560 with charge reduction by CAPTR. Smaller protein ions with lower masses, lower initial *m*/*z*
561 values, and lower initial Ω generally compacted more significantly with *C* than larger ions, as
562 evidenced by larger percent decreases in Ω with CAPTR, even over the same number of CAPTR
563 events (Figure 8A and 8C).
564 An exception to this trend was observed when comparing 18→8 ions of cytochrome *c* to
565 13→3 ions of lysozyme from DI conditions. Although these both correspond to 10 CAPTR
566 events, and the charge density is greater for 18+ ions of cytochrome *c* when compared to 13+
567 ions of lysozyme from DI conditions, lysozyme ions exhibited greater compaction in Ω (37% vs
568 30%). When we instead compare 13→3 ions from both proteins, cytochrome *c* ions exhibited the
569 greater compaction in Ω. There was a steeper decrease in Ω when subjecting the 13+ cytochrome
570 *c* precursor ions to 10 CAPTR events than when subjecting the 18+ ions to the same extent of

571 CAPTR. This may suggest that, up to a certain point, excess protons limit the formation of
572 additional noncovalent interactions because the Coulombic strain is still too high. Additionally,
573 13→*C* cytochrome *c* ions were similar in Ω to the 18→*C* ions where *C* = 13 to 3. An increase in
574 the rate of compaction with CAPTR was also observed for BSA ions from DISC and DRSC
575 conditions below *C* = 36, supporting this hypothesis. 18+ DI lysozyme ions were not observed
576 from denaturing conditions, so 18→*C* ions are not available for comparison; however, disulfide-
577 reduced (DR) lysozyme 18+ ions were produced and subjected to CAPTR. 18→*C* ions exhibited
578 similar extents of compaction to cytochrome *c* 18→*C* ions across all *C*. This observation
579 suggests that, in addition to charge density, other aspects of structure, *e.g.*, disulfide-bonding,
580 impact the relationship between Ω and charge.
581 The Ω values of native-like ions depended relatively weakly on charge (Figure 8B and
582 8D). Compared to denatured ions, the percent decrease in Ω values with CAPTR was minimal,
583 but a similar trend between charge density and the extent of compaction was observed. These
584 experiments suggest that the amount of charging resulting from ESI is generally well-
585 accommodated by large, native-like protein ions, but it can still have a modest effect on Ω. The
586 structures of smaller protein ions appear to be far more sensitive to the excess charges associated
587 with ESI.
588 Altogether, these observations reveal that excess charges can have a larger effect on
589 smaller protein ions, which may be the result of higher charge density, lower surface-to-volume
590 ratios, and a more limited ability to self-solvate those excess charges. These results are in
591 agreement with recent work investigating the charge-state distributions of protein ions formed by
592 ESI and their relationships with Ω (Rolland et al. 2022). Smaller protein ions exhibited more
593 positive slopes in Ω with increasing charge across their charge-state distributions. The increase

in Ω with charge was attributed to the limited ability of these smaller proteins to undergo surface compaction and self-solvation, leading to Coulombic repulsion that stabilized larger conformations (Rolland et al. 2022). This is consistent with the stronger relationship observed between Ω and *z* for smaller proteins using CAPTR-IM-MS. This suggests that smaller, native-like ions have significant Coulombic strains, which are associated with more significant decreases in Ω upon charge reduction, whereas larger, native-like ions initially have lower Coulombic strains, and concomitantly, exhibit less compaction upon charge reduction.

IV. Probing Energy Landscapes

Energy-dependent IM is used to study the stability and conformational space of ions in the gas phase (Pierson et al. 2010). For example, in collision-induced unfolding (CIU), native-like ions are activated as a function of collision energy and then analyzed by IM. Activation enables ions to overcome the energy barriers to isomerization and often results in the formation of new, stable structures that have larger Ω values (Dixit et al. 2018). CIU results have been used to study the stabilities of proteins (Freeke et al. 2012), modes of ligand binding (Rabuck et al. 2013), and to differentiate similar biotherapeutics (Tian et al. 2015). Applying collisional activation before or after CAPTR enables us to probe different regions of the energy landscapes of gas-phase ions.

A. Pre-CAPTR Activation

Pre-CAPTR activation is performed on precursor ions prior to subjecting them to CAPTR for charge reduction. This will be represented with an asterisk by the precursor charge state: $P^* \rightarrow C$. Pre-CAPTR activation can be accomplished at the atmospheric-pressure interface by

617 increasing the bias between the sampling cone voltage and the extraction cone (Figure 3C). Pre-
618 CAPTR activation has also been accomplished by increasing the bias between the quadrupole
619 and the trap cell (Laszlo et al. 2016). These methods allow for the investigation of the effects of
620 precursor activation on product ion structures and have been proposed to provide an indirect
621 probe of precursor ion structure. For example, in studying denatured ubiquitin ions with CAPTR,
622 the 8*→8 (activated precursor ions that did not undergo reaction) Ω distributions were
623 independent of the voltage applied (Laszlo et al. 2016), but the Ω distributions of the 8*→6 ions
624 changed with increasing energy (Figure 11E). The 8*→6 ions display features I, II, and III, with
625 I being the most intense at low energies. Features II and III grow in intensity, whereas feature I
626 decreases in intensity, with increasing activation. It is possible that the 8*→8 ions isomerize to
627 different conformations that have indistinguishable Ω, but form structures with resolvable Ω for
628 the 8*→6 ions. For the highest energies tested (70 to 100 V), the 8*→6 distributions were
629 similar. This may reflect a quasi-equilibrium (Pierson et al. 2010) of structures formed in the
630 8*→8 populations at those energies.
631 Recently, pre-CAPTR activation was used to differentiate IgG1κ and IgG4κ from human
632 myeloma (Gozzo & Bush, manuscript in preparation). These antibodies have high sequence
633 similarity and have the same number of interchain disulfide bonds, but they differ in connectivity
634 of said bonds (Vidarsson et al. 2014). They are difficult to differentiate by IM-MS alone (Tian et
635 al. 2015). The 25*→25 ions of IgG1 and IgG4 displayed indistinguishable or very similar Ω
636 distributions at all the pre-CAPTR activation voltages tested, but with charge reduction, the Ω
637 distributions of the 25*→12 ions were more resolved. At 75 V precursor activation, for example,
638 IgG4 did not compact as much as IgG1 with charge reduction, creating differences in the Ω
639 distributions with decreasing charge that reflect the subtle differences in their structures. These

results suggest that pre-CAPTR activation and IM-MS may be useful for differentiating similar biomolecules and biotherapeutics, even in cases where activation and IM-MS alone (*i.e.*, CIU) are inadequate.

B. Post-CAPTR Activation

Post-CAPTR activation is performed on residual precursor and CAPTR product ions after exiting the trap cell and before analysis by IM-MS. This is represented with an asterisk by the product charge state: $P \rightarrow C^*$. Post-CAPTR activation can be performed as a function of the dc bias between the trap cell and mobility cell, which increases the kinetic energy of ions during injection to the mobility cell (Figure 3C). Collisional activation after CAPTR also been accomplished by establishing a region analogous to the helium cell on the unmodified Synapt G2 (Giles et al. 2011), but pressurizing it with argon for more energetic collisions (Laszlo & Bush 2017). This region is located just prior to the drift region. Post-CAPTR activation is used to directly probe the stabilities and structures of product ions.

Post-CAPTR activation was applied to the 6+ ions generated from various precursors (P = 6, 8, and 13) of denatured ubiquitin (Laszlo et al. 2016). The 6*→6 and 6→6* results were similar, indicating similar activation mechanisms for pre- and post-CAPTR activation in the experiments (Figure 11A and 11D). Features I, II, and III were observed in the Ω distributions, with feature I being the most compact and feature III being the most unfolded. At low energies, 6→6* displayed mainly feature I, with low intensity for the other two features. 8→6* ions also exhibited the highest intensity for feature I, but presented significant intensities for features II and III as well. With increasing activation voltage, both the 6→6* and 8→6* ions unfolded to predominantly feature III, though 8→6* ions completed the transition 10 V earlier than 6→6*

663 ions (Figure 11A and 11B). In contrast, 13→6* ions populate feature II mainly, with low
664 intensities of I and III at low energies (Figure 11C). The intensity of feature I doesn't change
665 significantly with increasing energy but feature II gives way slightly and feature III increases in
666 intensity until they are about equivalent at the highest voltages. The persistence of features I and
667 II contrasts observations for the 6→6* and 8→6* ions, which suggests that 13→6* ions exhibit
668 different structures than those ions. They do not appear to interconvert in these experiments,
669 indicating that different regions of the energy landscape were probed.
670 Post-CAPTR activation was also applied to 15+ ions of BSA generated from different
671 solution conditions (Gadzuk-Shea & Bush 2018). In this case, nitrogen was used as the drift gas,
672 so, as ions were injected into the mobility cell with increasing voltage, more efficient energy
673 deposition occurred than with a helium-filled drift cell. 15→15* ions from NI conditions,
674 60→15* ions from DISC conditions, and 70→15* ions from DRSC were tested. The apparent Ω
675 distributions and their median values are presented in Figure 12. At low energies, Ω distributions
676 of ions from DRSC and DISC conditions overlapped significantly, while the Ω distributions of
677 ions from NI conditions were distinct and appeared at smaller Ω. With increasing activation, the
678 populations from DRSC and DISC conditions began to compact while the ions from NI
679 conditions got larger. At the highest injection voltages, ions generated from all three conditions
680 exhibited similar Ω values and their Ω distributions largely overlapped, providing evidence for
681 population of similar areas of their energy landscapes. The distributions of ions from DRSC were
682 slightly shifted to larger Ω compared to distributions of ions from NI and DISC conditions. This
683 is different from the results observed using post-CAPTR activation on ubiquitin 6+ ions
684 generated from the same solution conditions, but from different precursors (Laszlo et al. 2016).
685 In this case, a quasi-equilibrium (Pierson et al. 2010) of structures may have been reached before

686 the energy required for dissociation was reached. On the other hand, these ions could have
687 different structures that just happen to coincide in Ω. The initial population of 15+ ions from NI
688 conditions is significantly different than the other populations based on its response to increasing
689 energy; the ions from NI conditions overcome energy barriers to isomerize to larger structures
690 while the other ions decrease in size. This reflects the disintegration of intramolecular
691 interactions that prevent such expansion, whereas the compaction of ions from DISC and DRSC
692 conditions may be credited to the formation of initially absent intramolecular interactions. This
693 provides additional support for the generation of kinetically trapped structures via ESI; ions from
694 different solution conditions retain aspects of condensed-phase structure, but gas-phase
695 equilibrium structures may be significantly different.
696
697 **V. Comparison to Results from Other Charge-Reduction Strategies**
698 The following section compares the IM-MS results from studies using CAPTR with those
699 using other methods to manipulate charge. As discussed in the *Charge Manipulation* section,
700 these methods include the addition of solution modifiers prior to ESI, atmospheric-pressure
701 methods, gas-phase ion/neutral chemistry, and gas-phase ion/ion chemistry. Some methods
702 include the isolation of precursors of a specific charge state, but others simultaneously affect all
703 precursors. This discussion focuses on studies of ubiquitin, cytochrome *c*, lysozyme, alcohol
704 dehydrogenase, and pyruvate kinase. Although many of these studies used drift tubes (Gabelica
705 et al. 2019) or radio-frequency confining drift tubes (Allen & Bush 2016) containing helium gas,
706 some used traveling-wave IM in N_2 gas and external calibration with helium-based Ω values. We
707 will not discuss potential bias in the values determined using the latter, but the challenges and

potential errors associated with calibration are discussed elsewhere (Bush et al. 2010, 2012; Zhong et al. 2011).

A. Effects of Charge on Small, Single-Domain Proteins

Ubiquitin and cytochrome *c* are widely used as models of single-domain proteins. Results from the following experiments were selected for comparison to results from CAPTR of these protein ions: ion/neutral proton transfer of denatured ubiquitin (Valentine et al. 1997b), crETD of denatured ubiquitin (Lermyte et al. 2017), and crETD of native-like and denatured cytochrome *c* (Jhingree et al. 2017). CAPTR was performed on quadrupole-selected 6+ to 13+ ubiquitin ion populations generated from denaturing solution conditions, as discussed in the *CAPTR of Proteins from Denaturing Solutions* section and shown in Figure 5 (Laszlo et al. 2016). Clemmer and coworkers generated ubiquitin ions from a different denaturing solution and performed ion/neutral proton-transfer reactions broadly, on the whole population of observed ions, 6+ to 13+ (Valentine et al. 1997b). Results of ion/neutral proton-transfer reactions are shown in Figure 2. $^{DT}\Omega_{He}$ values of the precursor ions in these two studies were similar, with some differences observed for 6+ to 8+ distributions. After CAPTR, all $P \rightarrow C$ ions exhibited smaller Ω values than their precursors (Laszlo et al. 2016). The product ions of a particular *C* formed from different *P* had very similar Ω values, pointing to a strong dependence on *P* and a weak dependence on *C*. These results are also consistent with an earlier study of ion/ion proton transfer of ubiquitin ions (Zhao et al. 2009).

The 4+ and 5+ products of ion/neutral proton transfer from ubiquitin cations to different bases exhibited either compact or partially folded, rather than elongated conformers (Valentine et al. 1997b). More-compact populations were depleted preferentially; this effect was stronger with

stronger bases. More-elongated populations exhibited no evidence for folding, which was attributed to the larger gas-phase acidities of elongated protein ions (*i.e.*, removing a proton from those ions is more endergonic) and the preferential depletion of compact ions that are expected to have smaller gas-phase acidities (Valentine et al. 1997b) (*i.e.*, removing a proton from those ions is less endergonic). In contrast, CAPTR appears to charge reduce all conformers of ubiquitin (Laszlo et al. 2016), which is consistent with the large exergonicity of ion/ion proton-transfer reactions. Despite these differences, both studies report Ω values that depend strongly on *z*.

CAPTR (Laszlo et al. 2016) and crETD (Lermyte et al. 2017) of selected ubiquitin ions generated from denaturing solutions both resulted in folding and compaction in Ω with charge reduction. crETD was performed on quadrupole-selected ubiquitin ions with 1,4-dicyanobenzene radical anions (Lermyte et al. 2015, 2017); this reagent yields both proton-transfer and electron-transfer products (Gunawardena et al. 2005; Liu & McLuckey 2012; McLuckey & Stephenson 1998). In this case, the apparent ratio of proton-transfer to electron-transfer products was determined, and, in contrast to ion/neutral studies, preferential depletion of certain conformations was not observed, which was attributed to the more homogenous sizes of the precursor ions. In both the crETD and CAPTR studies, the charge-reduced products exhibited similar Ω values to those for the identically charged ions generated directly from ESI, indicating that Ω depends on *z*. With increasing post-reduction collisional activation, the Ω distributions of 6→6* and 8→6* ions evolved qualitatively similarly in the two studies, suggesting similar structures may have been probed.

CAPTR was performed on quadrupole-selected cytochrome *c* ions generated from both native-like and denaturing solution conditions as discussed earlier and shown in Figure 6 (Laszlo et al. 2017a). crETD was performed on quadrupole-selected cytochrome *c* ions from similar

754 solution conditions using 1,3-dicyanobenzene radical anions (Jhingree et al. 2017). That study
755 reports that proton transfer was not a major pathway in those crETD experiments. Like the
756 ion/neutral studies of denatured ubiquitin, the most compact features of denatured cytochrome *c*
757 were preferentially depleted by charge-reduction reactions; the remaining precursor ions
758 exhibited more extended populations. In CAPTR experiments, preferential depletion was not
759 observed. Despite some differences in precursor and product distributions, both studies observed
760 that Ω depended on *z*. For instance, 10+ products of crETD from 10+, 11+, and 12+ precursor
761 ions all exhibited similar Ω distributions (Jhingree et al. 2017). For the intermediate-charged
762 CAPTR products ($P \rightarrow C$, C = 9 to 5), the Ω of the product ions also depended weakly on P
763 (Laszlo et al. 2017a). Ω distributions of native-like ions generated for CAPTR experiments were
764 significantly smaller and exhibited fewer features than the corresponding native-like ions in
765 crETD studies. To perform crETD in this case, the optimized instrument conditions were
766 activating. When crETD was performed on the native-like 7+ ions for example, the resulting 6+
767 ions compacted to sizes closer to native-like 6+ ions measured under non-crETD conditions
768 (Jhingree et al. 2017). As a result, compaction was more significant than was observed with
769 CAPTR. Overall, these studies suggest that Ω can depend strongly on *z* for small, single-domain
770 protein cations.
771
772 **B. Effects of Charge on Proteins with Internal Disulfide Bonds**
773 Lysozyme is a 14 kDa protein whose native structure contains four internal disulfide
774 bonds. The charge states of lysozyme ions from denaturing, disulfide-intact (DI) and denaturing,
775 disulfide-reducing (DR) conditions have been manipulated using ion/neutral proton transfer
776 reactions (Valentine et al. 1997a) and CAPTR (Laszlo et al. 2017b). Both studies reported

similar $^{DT}\Omega_{He}$ values for ions from DR conditions and the presence of a slightly unfolded population for ions from DI conditions, but the earlier study also reported a more-folded population for ions from DI conditions. For the ion/neutral proton-transfer experiments, the full populations of lysozyme ions from DI or DR conditions were transmitted through a gas cell containing a vapor of either n-butylamine or 7-methyl-1,5,7-triazobicyclo[4.4.0]dec-5-ene (Valentine et al. 1997a). For ions from both conditions that were subjected to ion/neutral proton-transfer reactions, $^{DT}\Omega_{He}$ distributions were more compact than those of the originating ions (Valentine et al. 1997a). CAPTR of selected precursors from both conditions also yielded charge-reduced product ions that were more compact than their precursors (Laszlo et al. 2017b).

Energy-dependent experiments were used to probe stabilities of charge-reduced lysozyme ions. For ions from DI conditions, collisional activation of 6+ lysozyme ions from ion/neutral proton transfer resulted in $^{DT}\Omega_{He}$ values that appeared to be independent of the applied activation voltage (Valentine et al. 1997a). In contrast, the $^{DT}\Omega_{He}$ values of 12→6* CAPTR products decreased with increasing energy (Laszlo et al. 2017b). At low energies, the 12→6* ions exhibited $^{DT}\Omega_{He}$ values that were larger than those of the 6+ ions from ion/neutral proton transfer, and at the highest energies, 12→6* ions exhibited $^{DT}\Omega_{He}$ values that were indistinguishable from those of the 6+ ions from ion/neutral proton transfer (Laszlo et al. 2017b; Valentine et al. 1997a). The results are consistent with the formation of fully annealed products following ion/neutral proton-transfer reactions and kinetically trapped products following CAPTR; with increasing energy the CAPTR products anneal and have similar structures to those formed directly by ion/neutral proton-transfer reactions. Potential factors that may contribute to these results include: (1) the CAPTR product was generated from a 12+ precursor, whereas the ion/neutral proton-transfer products were generated from a full distribution of charge states that

800 did not extend to the 12+ ion, (2) ion/neutral proton-transfer products may have preferentially
801 reacted with more compact precursors and yielded more compact products (Valentine et al.
802 1997b), and (3) ion/neutral proton-transfer may result in greater heating (and pre-annealing) than
803 CAPTR.

804 For ions from DR conditions, collisional activation of 6+ lysozyme ions from ion/neutral
805 proton transfer resulted in $^{DT}\Omega_{He}$ values that increased with increasing energy (Valentine et al.
806 1997a). At low energies, the 12→6* CAPTR products exhibited larger $^{DT}\Omega_{He}$ values than those
807 for the 6+ ions from ion/neutral proton transfer. With increasing energy, structures with smaller
808 $^{DT}\Omega_{He}$ values became populated, but larger structures near 17.5 nm^2 persisted over all energies.
809 Although the results from these two studies using identical DR conditions indicate that Ω can
810 depend strongly on *z* and the presence of disulfide bond, the significant differences in the energy-
811 dependent IM analysis of ions from ion/neutral proton-transfer reactions and CAPTR suggest
812 that those two charge-reduction methods can yield products that populate very different regions
813 of the energy landscape of a protein.
814

815 **C. Effects of Charge on Native-Like Ions of Larger Proteins**

816 Alcohol dehydrogenase (ADH) and pyruvate kinase (PK), which are homotetramers with
817 masses of 147 and 237 kDa respectively, have been used to study the effects of charge on the
818 structures of native-like protein ions. In addition to CAPTR (Laszlo & Bush 2017), the charge
819 states of ADH and PK have been manipulated using solution-phase additives of triethylamine
820 (Allen et al. 2013) or 1,5-diazabicyclo[4,3,0]non-5-ene (DBU) (Bornschein et al. 2011), and
821 ion/neutral proton transfer with nebulized DBU (Bornschein et al. 2011). In addition, the charge
822 states of ADH have been manipulated using crETD with 1,4-dicyanobenzene radical anions

(Lermyte et al. 2015) and those of PK have been manipulated using corona-discharge (Campuzano & Schnier 2013). CAPTR and crETD were applied to quadrupole-selected ions, whereas other charge-reduction methods were applied to all ions simultaneously.

Figure 13A shows Ω values of ADH as a function of charge state. Overall, CAPTR yielded the widest range of product-ion charge states. The products compacted slightly following the first few CAPTR events and the maximum decrease in Ω relative to the precursor was 3.6% (Laszlo & Bush 2017). Ω values of ions generated from solutions with triethylamine were nearly identical to those of ions of the same *z* from native-like conditions (Allen et al. 2013). Below 24+, ions generated from triethylamine solution increased in Ω modestly with decreasing charge (Allen et al. 2013). A similar trend was observed for ions exposed to nebulized DBU at atmospheric pressure (Bornschein et al. 2011). When DBU was added to solution, instead of introduced in the gas phase, addition activation was required to knock off proton-bound base molecules and accomplish the desired charge reduction (Bornschein et al. 2011). This also resulted in slightly unfolded ions that were significantly larger than native-like ions from ESI at charge states 21+ to 27+. These ions exhibited a significant decrease in Ω with decreasing charge state. The observation that solution modifiers often complex with protein cations during ESI – thus requiring supplemental activation to release the protein ion of interest – illustrates some of the challenges associated with using solution modifiers and using the resulting data to understand the relationship between charge and protein ion structure. The Ω values of crETD products of ADH depended more strongly on charge state than those for the CAPTR products, *e.g.*, the 26+ precursor yielded a 15+ product that was 6.4% smaller (Lermyte et al. 2015). The comparatively large decrease in Ω when 26+ ADH is subjected to crETD is consistent with heating and annealing of those products; the arrival times of 25→17* ADH ions decrease with increasing

post-CAPTR collision energy (Laszlo & Bush 2017). The products generated from crETD may be different than those produced from CAPTR; charge reduction with 1,4-dicyanobenzene radical anions can proceed through either non-dissociative electron transfer or proton transfer. All studies of the charge reduction of native-like ions of ADH indicate the Ω values of these ions depend less strongly on charge than smaller, single-domain proteins.

Figure 13B shows Ω values as a function of charge state for PK. For experiments with DBU and triethylamine, similar challenges were reported as described above for ADH (Allen et al. 2013; Bornschein et al. 2011). Incorporating triethylamine into the electrospray solution and exposing ions to nebulized DBU both yielded ions with Ω values that were similar to those generated from solutions without those modifiers (Allen et al. 2013; Bornschein et al. 2011). These results support the claim that the structure of native-like PK ions does not depend strongly on charge state. Another study generated PK ions from native-like conditions in close proximity to a corona-discharge probe using N_2 gas (Campuzano & Schnier 2013). Contrary to results using the other approaches discussed, the application of the corona-discharge probe yields ions whose Ω values decrease significantly with decreasing *z*, *e.g.*, the Ω values of the 25+ ions were 19% smaller than the 36+ ions (Campuzano & Schnier 2013). These differences may be attributable to factors inherent to the charge-reduction method, *e.g.*, generation of new species by corona discharge or activation in the high fields of the discharge region. Alternatively, the larger changes reported for these experiments could be a consequence of the IM measurement, which used traveling-wave IM with ramped amplitudes.

VII. Energetics

As discussed in the section *Manipulating the Charge States of Protein Ions*, ion-ion reactions like CAPTR (Reaction 3) are expected to be highly exothermic. These expectations originate from comparison of the proton affinities of the monoanion and the protein cations (McLuckey & Stephenson 1998). Here, we will expand on energetics by quantifying the change in free energy of these reactions, and we will discuss implications for interpreting CAPTR data. Reaction 3 can be separated into reactions for extracting a proton from a protein polycation:

$$[M + xH]^{x+} \rightarrow [M + (x-1)H]^{(x-1)+} + H^+ \quad (6)$$

and adding a proton to the monoanion:

$$[PDCH - F]^- + H^+ \rightarrow [PDCH - F + H] \quad (7)$$

The change in free energy for a proton-transfer reaction in the gas phase is usually expressed using the gas-phase basicity (GB) of the proton acceptor, which is the negative of the change in free energy that occurs when the proton acceptor and a proton combine to form product. Therefore, the change in free energies for Reactions 6 and 7 are:

$$\Delta G_{Reaction\,5} = GB([M + (x-1)H]^{(x-1)+}) \quad (8)$$

$$\Delta G_{Reaction\,6} = -GB([PDCH - F]^-) \quad (9)$$

Experimental measurements of the apparent GB of cytochrome *c* ions generated from denaturing solutions range from 801 kJ mol^{-1} (for the 15+ ion) to 980 kJ mol^{-1} (for the 3+ ion) (Schnier et al. 1995); GB values increase with decreasing charge state. Based on experimental measurements of the GB of lysine-containing peptide ions (Schnier et al. 1995; Sterner et al. 1999) and the relative GB of lysine and arginine (Bouchoux 2012), we proposed an upper limit for the GB of a protein ion of 1080 kJ mol^{-1} (Laszlo & Bush 2015). Based on electronic structure calculations, the diabatic GB of the lowest-energy conformer of [PDCH–F]$^-$ was 1310 kJ mol^{-1}. Many

conformers of the reactant and product were also considered, but this was the smallest GB found for this reaction (Laszlo & Bush 2015).

These comparisons suggest that each CAPTR event is exergonic by at least 230 kJ mol^{-1}, as shown in Figure 14. A protein ion has far more degrees of freedom than the PDCH–containing product, therefore statistical partitioning of the energy from a series of CAPTR events would result in significant heating of the protein ion. However, no significant fragmentation has been observed during CAPTR experiments (Laszlo & Bush 2015), which is consistent with analogous reactions performed under different conditions (Stephenson et al. 1997). Furthermore, activation and re-thermalization of CAPTR products can result in the formation of new structures (see the *Post-CAPTR Activation* section). Those results indicate that the structures of CAPTR products depend strongly on kinetic trapping, *i.e.*, energy deposition during CAPTR is insufficient to anneal the products and form the equilibrium distribution of structures.

Although the total change in free energy resulting from each CAPTR event is highly exergonic, it is possible that the energy does not partition statistically between the products. For example, Uggerud and coworkers reported results from *ab initio* direct dynamics of proton transfer from the hydronium cation to neutral ammonia (Bueker et al. 1996) In some trajectories, the proton transferred directly and deposited a "high and nonstatistical fraction of the reaction enthalpy into the product ammonium ion." In trajectories exhibiting long-lived interaction complexes, the reaction enthalpy partitioned statistically between the products (Bueker et al. 1996). Because the rate-limiting step of ion/ion reactions in the gas phase is the formation of a long-range interaction complex (Gunawardena et al. 2005), direct proton transfer and nonstatistical partitioning may be even more likely for ion/ion reactions than for the ion/neutral reaction considered by Uggerud and coworkers.

913 Based on the evidence and discussion above, we propose that nonstatistical partitioning
914 of energy into the neutralized monoanion is a significant process during CAPTR experiments,
915 which would result in significantly less heating of charge-reduced protein ions than suggested by
916 the large total change in free energy associated with each CAPTR event. Although some
917 interpretations of ECD and ETD data invoke nonstatistical partitioning of energy after the
918 polycation combines with an electron (Breuker et al. 2004; Leib et al. 2007), all models are
919 consistent with the bulk of that recombination energy being available to the reduced cation
920 (Syrstad & Turecček 2005; Turecček et al. 2008; Tureček & Julian 2013). Note that in ECD, a
921 free electron combines with a polycation; without fragmentation the entire recombination energy
922 must partition into the protein. In ETD, extracting an electron from a monoanion is endergonic
923 and combining that electron with the polycation is exergonic; it is challenging to envision a
924 mechanism for the exergonicity of that reaction to preferentially partition into the electron donor.
925 Therefore, relative to CAPTR, electron-based, charge-reduction methods result in greater energy
926 deposition into the charge-reduced protein ions. The extent of ion heating from this energy
927 deposition will be mitigated by the large number of degrees of freedom of protein ions and
928 competition with relaxation via radiative emission and collisional cooling.
929
930 **VII. Conclusions**
931 Foundational IM-MS studies demonstrated that protein ions with different charge states
932 can exhibit very different **Ω** values (Figure 2). However, the charge states observed for a given
933 protein can depend on many factors (Figure 1), not all of which affect their **Ω** values. Combining
934 charge manipulation and IM-MS has furthered our understanding of the relationship between the
935 charge states and structures of protein ions in the gas phase. Results from CAPTR-IM-MS

experiments on a variety of protein ions suggest that charge density plays a crucial role in this relationship. Protein ions with higher charge densities, *i.e.*, smaller *m*/*z* values, generally experience significant decreases in Ω values following each CAPTR event (Figure 8C). For these protein ions, the charge state appears to be a predominant factor affecting their gas-phase structure (Figures 5, 6A, and 7A-C). On the other hand, protein ions with low charge densities tend to have Ω values that depend weakly on charge state (Figure 8D), suggesting that their gas-phase structure is not primarily determined by charge state and corroborating their ability to retain many structural characteristics from solution (Figures 6B, 7D, and 10). Other factors influencing the magnitude of the decreases in Ω values following CAPTR events include the original solution conditions prior to ESI and the presence of disulfide bonds (Figure 7). Compared to other charge-manipulation strategies, CAPTR-IM-MS experiments offer the advantage of precursor isolation (Figure 3) and the ability to analyze a large series of charge-reduced products in parallel (Figure 4).

Activating CAPTR precursors, *i.e.*, pre-CAPTR activation, or CAPTR products, *i.e.*, post-CAPTR activation (Figure 3C), often results in the formation of new structures that have different Ω values (Figures 11 and 12). This indicates that CAPTR products are kinetically trapped and can retain a memory of their solution-phase structures. The observed kinetic trapping and lack of fragmentation, despite the high net exergonicity of each CAPTR event (Figure 14), suggests that energy partitions preferentially into the neutralized monoanion. This may limit the structural changes to the portions that interacted with the extracted charge. Compared to other charge-reduction strategies, CAPTR-IM-MS appears to offer more independent control over the extent of charge reduction and energy deposition during experiments. CAPTR also exhibits no signs of selective reaction with certain precursor conformations over others.

CAPTR-IM-MS has proven to be an effective method for unraveling the complex relationship between the charge state and structure of protein ions. With the ability to isolate the contributions of charge from other factors, this technique offers a valuable addition to the current suite of tools for structural biology and biophysics research. Its ability to resolve charge-state ambiguities (Figure 4) and enhance the resolution of ions with similar m/z values (Equation 5) provides a clear advantage for native mass spectrometry. We suggest that researchers consider incorporating CAPTR into their workflows when exploring the structures of proteins and their complexes.

Acknowledgements

This work was supported by the National Science Foundation through award 2203513 from the Division of Chemistry, with partial co-funding from the Division of Molecular and Cellular Biosciences. The entire Bush lab and its alumni want to thank and gratefully acknowledge Prof. František Tureček. As a collaborator and colleague, he helped inspire our interest in combining ion-ion chemistry and IM-MS, facilitated the integration of ion-ion chemistry on our first IM-MS system, and most importantly, helped us all do our best science.

975 **References**

976 Abzalimov RR, Kaltashov IA. 2010. Electrospray Ionization Mass Spectrometry of Highly
977 Heterogeneous Protein Systems: Protein Ion Charge State Assignment via Incomplete
978 Charge Reduction. *Anal. Chem.* 82(18):7523–26

979 Allen SJ, Bush MF. 2016. Radio-Frequency (rf) Confinement in Ion Mobility Spectrometry:
980 Apparent Mobilities and Effective Temperatures. *J. Am. Soc. Mass Spectrom.*
981 27(12):2054–63

982 Allen SJ, Giles K, Gilbert T, Bush MF. 2016. Ion mobility mass spectrometry of peptide, protein,
983 and protein complex ions using a radio-frequency confining drift cell. *The Analyst*.
984 141(3):884–91

985 Allen SJ, Schwartz AM, Bush MF. 2013. Effects of Polarity on the Structures and Charge States
986 of Native-Like Proteins and Protein Complexes in the Gas Phase. *Anal. Chem.*
987 85(24):12055–61

988 Barth M, Schmidt C. 2020. Native mass spectrometry—A valuable tool in structural biology. *J.*
989 *Mass Spectrom.* 55(10):

990 Benesch JLP, Ruotolo BT, Sobott F, Wildgoose J, Gilbert A, et al. 2009. Quadrupole-Time-of-
991 Flight Mass Spectrometer Modified for Higher-Energy Dissociation Reduces Protein
992 Assemblies to Peptide Fragments. *Anal. Chem.* 81(3):1270–74

993 Bleiholder C, Johnson NR, Contreras S, Wyttenbach T, Bowers MT. 2015. Molecular Structures
994 and Ion Mobility Cross Sections: Analysis of the Effects of He and N_2 Buffer Gas. *Anal.*
995 *Chem.* 87(14):7196–7203

996 Bleiholder C, Liu FC. 2019. Structure Relaxation Approximation (SRA) for Elucidation of
997 Protein Structures from Ion Mobility Measurements. *J. Phys. Chem. B*. 123(13):2756–69

998 Bohrer BC, Merenbloom SI, Koeniger SL, Hilderbrand AE, Clemmer DE. 2008. Biomolecule
999 Analysis by Ion Mobility Spectrometry. *Annu. Rev. Anal. Chem.* 1(1):293–327
1000 Bornschein RE, Hyung S-J, Ruotolo BT. 2011. Ion Mobility-Mass Spectrometry Reveals
1001 Conformational Changes in Charge Reduced Multiprotein Complexes. *J. Am. Soc. Mass*
1002 *Spectrom.* 22(10):s13361-011-0204-y
1003 Bouchoux G. 2012. Gas phase basicities of polyfunctional molecules. Part 3: Amino acids. *Mass*
1004 *Spectrom. Rev.* 31(3):391–435
1005 Breuker K, Oh H, Lin C, Carpenter BK, McLafferty FW. 2004. Nonergodic and conformational
1006 control of the electron capture dissociation of protein cations. *Proc. Natl. Acad. Sci.*
1007 101(39):14011–16
1008 Bueker H-H, Helgaker T, Ruud K, Uggerud E. 1996. Energetics and Dynamics of Intermolecular
1009 Proton-Transfer Processes. 2. Ab Initio Direct Dynamics Calculations of the Reaction $H_3O^+ + NH_3 \rightarrow NH_4^+ + H_2O$. *J. Phys. Chem.* 100(38):15388–92
1011 Bush MF, Campuzano IDG, Robinson CV. 2012. Ion Mobility Mass Spectrometry of Peptide
1012 Ions: Effects of Drift Gas and Calibration Strategies. *Anal. Chem.* 84(16):7124–30
1013 Bush MF, Hall Z, Giles K, Hoyes J, Robinson CV, Ruotolo BT. 2010. Collision Cross Sections
1014 of Proteins and Their Complexes: A Calibration Framework and Database for Gas-Phase
1015 Structural Biology. *Anal. Chem.* 82(22):9557–65
1016 Campuzano IDG, Schnier PD. 2013. Coupling electrospray corona discharge, charge reduction
1017 and ion mobility mass spectrometry: From peptides to large macromolecular protein
1018 complexes. *Int. J. Ion Mobil. Spectrom.* 16(1):51–60
1019 Canzani D, Laszlo KJ, Bush MF. 2018. Ion Mobility of Proteins in Nitrogen Gas: Effects of
1020 Charge State, Charge Distribution, and Structure. *J. Phys. Chem. A*. 122(25):5625–34

1021 Cheung See Kit M, Webb IK. 2022. Application of Multiple Length Cross-linkers to the
1022 Characterization of Gaseous Protein Structure. *Anal. Chem.* 94(39):13301–10
1023 Clemmer DE, Hudgins RR, Jarrold MF. 1995. Naked Protein Conformations: Cytochrome c in
1024 the Gas Phase. *J. Am. Chem. Soc.* 117(40):10141–42
1025 Dixit SM, Polasky DA, Ruotolo BT. 2018. Collision induced unfolding of isolated proteins in the
1026 gas phase: past, present, and future. *Curr. Opin. Chem. Biol.* 42:93–100
1027 Ebeling DD, Westphall MS, Scalf M, Smith LM. 2000. Corona Discharge in Charge Reduction
1028 Electrospray Mass Spectrometry. *Anal. Chem.* 72(21):5158–61
1029 Freeke J, Bush MF, Robinson CV, Ruotolo BT. 2012. Gas-phase protein assemblies: Unfolding
1030 landscapes and preserving native-like structures using noncovalent adducts. *Chem. Phys.*
1031 *Lett.* 524:1–9
1032 Gabelica V, Shvartsburg AA, Afonso C, Barran P, Benesch JLP, et al. 2019. Recommendations
1033 for reporting ion mobility Mass Spectrometry measurements. *Mass Spectrom. Rev.*
1034 38(3):291–320
1035 Gadzuk-Shea MM, Bush MF. 2018. Effects of Charge State on the Structures of Serum Albumin
1036 Ions in the Gas Phase: Insights from Cation-to-Anion Proton-Transfer Reactions, Ion
1037 Mobility, and Mass Spectrometry. *J. Phys. Chem. B*. 122(43):9947–55
1038 Geels RBJ, van der Vies SM, Heck AJR, Heeren RMA. 2006. Electron Capture Dissociation as
1039 Structural Probe for Noncovalent Gas-Phase Protein Assemblies. *Anal. Chem.*
1040 78(20):7191–96
1041 Giles K, Williams JP, Campuzano I. 2011. Enhancements in travelling wave ion mobility
1042 resolution: Enhancements in travelling wave ion mobility resolution. *Rapid Commun.*
1043 *Mass Spectrom.* 25(11):1559–66

1044 Guilhaus M. 1995. Special feature: Tutorial. Principles and instrumentation in time-of-flight
1045 mass spectrometry. Physical and instrumental concepts. *J. Mass Spectrom.* 30(11):1519–
1046 32
1047 Gunawardena HP, He M, Chrisman PA, Pitteri SJ, Hogan JM, et al. 2005. Electron Transfer
1048 versus Proton Transfer in Gas-Phase Ion/Ion Reactions of Polyprotonated Peptides. *J.*
1049 *Am. Chem. Soc.* 127(36):12627–39
1050 Han Z, Chen LC. 2022. High-pressure nanoESI of highly conductive volatile and non-volatile
1051 buffer solutions from a large Taylor cone: Effect of spray current on charge state
1052 distribution. *Int. J. Mass Spectrom.* 476:116845
1053 He M, Emory JF, McLuckey SA. 2005. Reagent Anions for Charge Inversion of
1054 Polypeptide/Protein Cations in the Gas Phase. *Anal. Chem.* 77(10):3173–82
1055 Herron WJ, Goeringer DE, McLuckey SA. 1995. Gas-Phase Electron Transfer Reactions from
1056 Multiply-Charged Anions to Rare Gas Cations. *J. Am. Chem. Soc.* 117(46):11555–62
1057 Herron WJ, Goeringer DE, McLuckey SA. 1996. Product Ion Charge State Determination via
1058 Ion/Ion Proton Transfer Reactions. *Anal. Chem.* 68(2):257–62
1059 Hogan CJ, Carroll JA, Rohrs HW, Biswas P, Gross ML. 2009. Combined Charged Residue-Field
1060 Emission Model of Macromolecular Electrospray Ionization. *Anal. Chem.* 81(1):369–77
1061 Hogan CJ, Ruotolo BT, Robinson CV, Fernandez de la Mora J. 2011. Tandem Differential
1062 Mobility Analysis-Mass Spectrometry Reveals Partial Gas-Phase Collapse of the GroEL
1063 Complex. *J. Phys. Chem. B*. 115(13):3614–21
1064 Iavarone AT, Williams ER. 2003. Mechanism of Charging and Supercharging Molecules in
1065 Electrospray Ionization. *J. Am. Chem. Soc.* 125(8):2319–27

1066 Ikonomou MG, Kebarle P. 1992. An ion source with which ions produced by electrospray can be
1067 subjected to ion/molecule reactions at intermediate pressures (10–100 Torr).
1068 Deprotonation of polyprotonated peptides. *Int. J. Mass Spectrom. Ion Process.* 117:283–
1069 98
1070 Jhingree JR, Beveridge R, Dickinson ER, Williams JP, Brown JM, et al. 2017. Electron transfer
1071 with no dissociation ion mobility–mass spectrometry (ETnoD IM-MS). The effect of
1072 charge reduction on protein conformation. *Int. J. Mass Spectrom.* 413:43–51
1073 Jurneczko E, Barran PE. 2011. How useful is ion mobility mass spectrometry for structural
1074 biology? The relationship between protein crystal structures and their collision cross
1075 sections in the gas phase. *The Analyst*. 136(1):20–28
1076 Kafader JO, Melani RD, Schachner LF, Ives AN, Patrie SM, et al. 2020. Native vs Denatured:
1077 An in Depth Investigation of Charge State and Isotope Distributions. *J. Am. Soc. Mass*
1078 *Spectrom.* 31(3):574–81
1079 Kaiser RE, Louris JN, Amy JW, Cooks RG, Hunt DF. 1989. Extending the mass range of the
1080 quadrupole ion trap using axial modulation. *Rapid Commun. Mass Spectrom.* 3(7):225–
1081 29
1082 Kaldmäe M, Österlund N, Lianoudaki D, Sahin C, Bergman P, et al. 2019. Gas-Phase Collisions
1083 with Trimethylamine- *N* -Oxide Enable Activation-Controlled Protein Ion Charge
1084 Reduction. *J. Am. Soc. Mass Spectrom.* 30(8):1385–88
1085 Kaltashov IA, Mohimen A. 2005. Estimates of Protein Surface Areas in Solution by Electrospray
1086 Ionization Mass Spectrometry. *Anal. Chem.* 77(16):5370–79
1087 Kebarle P, Verkerk UH. 2009. Electrospray: From ions in solution to ions in the gas phase, what
1088 we know now. *Mass Spectrom. Rev.* 28(6):898–917

1089 Konermann L, Ahadi E, Rodriguez AD, Vahidi S. 2013. Unraveling the Mechanism of
1090 Electrospray Ionization. *Anal. Chem.* 85(1):2–9
1091 Laszlo KJ, Buckner JH, Munger EB, Bush MF. 2017a. Native-Like and Denatured Cytochrome *c*
1092 Ions Yield Cation-to-Anion Proton Transfer Reaction Products with Similar Collision
1093 Cross-Sections. *J. Am. Soc. Mass Spectrom.* 28(7):1382–91
1094 Laszlo KJ, Bush MF. 2015. Analysis of Native-Like Proteins and Protein Complexes Using
1095 Cation to Anion Proton Transfer Reactions (CAPTR). *J. Am. Soc. Mass Spectrom.*
1096 26(12):2152–61
1097 Laszlo KJ, Bush MF. 2017. Interpreting the Collision Cross Sections of Native-like Protein Ions:
1098 Insights from Cation-to-Anion Proton-Transfer Reactions. *Anal. Chem.* 89(14):7607–14
1099 Laszlo KJ, Munger EB, Bush MF. 2016. Folding of Protein Ions in the Gas Phase after Cation-
1100 to-Anion Proton-Transfer Reactions. *J. Am. Chem. Soc.* 138(30):9581–88
1101 Laszlo KJ, Munger EB, Bush MF. 2017b. Effects of Solution Structure on the Folding of
1102 Lysozyme Ions in the Gas Phase. *J. Phys. Chem. B*. 121(13):2759–66
1103 Leib RD, Donald WA, Bush MF, O'Brien JT, Williams ER. 2007. Nonergodicity in electron
1104 capture dissociation investigated using hydrated ion nanocalorimetry. *J. Am. Soc. Mass*
1105 *Spectrom.* 18(7):1217–31
1106 Lermyte F, Łącki MK, Valkenborg D, Gambin A, Sobott F. 2017. Conformational Space and
1107 Stability of ETD Charge Reduction Products of Ubiquitin. *J. Am. Soc. Mass Spectrom.*
1108 28(1):69–76
1109 Lermyte F, Williams JP, Brown JM, Martin EM, Sobott F. 2015. Extensive Charge Reduction
1110 and Dissociation of Intact Protein Complexes Following Electron Transfer on a
1111 Quadrupole-Ion Mobility-Time-of-Flight MS. *J. Am. Soc. Mass Spectrom.* 26(7):1068–76

Liu J, McLuckey SA. 2012. Electron transfer dissociation: Effects of cation charge state on product partitioning in ion/ion electron transfer to multiply protonated polypeptides. *Int. J. Mass Spectrom.* 330–332:174–81

Lomeli SH, Peng IX, Yin S, Ogorzalek Loo RR, Loo JA. 2010. New reagents for increasing ESI multiple charging of proteins and protein complexes. *J. Am. Soc. Mass Spectrom.* 21(1):127–31

Loo RRO, Udseth HR, Smith RD. 1991. Evidence of charge inversion in the reaction of singly charged anions with multiply charged macroions. *J. Phys. Chem.* 95(17):6412–15

Lyu J, Liu Y, McCabe JW, Schrecke S, Fang L, et al. 2020. Discovery of Potent Charge-Reducing Molecules for Native Ion Mobility Mass Spectrometry Studies. *Anal. Chem.* 92(16):11242–49

Marek A, Pepin R, Peng B, Laszlo KJ, Bush MF, Tureček F. 2013. Electron Transfer Dissociation of Photolabeled Peptides. Backbone Cleavages Compete with Diazirine Ring Rearrangements. *J. Am. Soc. Mass Spectrom.* 24(11):1641–53

Marek A, Shaffer CJ, Pepin R, Slováková K, Laszlo KJ, et al. 2015. Electron Transfer Reduction of the Diazirine Ring in Gas-Phase Peptide Ions. On the Peculiar Loss of [NH_4O] from Photoleucine. *J. Am. Soc. Mass Spectrom.* 26(3):415–31

Mason E, McDaniel W. 1988. *Transport Properties of Ions in Gases*. Wiley

McKay AR, Ruotolo BT, Ilag LL, Robinson CV. 2006. Mass Measurements of Increased Accuracy Resolve Heterogeneous Populations of Intact Ribosomes. *J. Am. Chem. Soc.* 128(35):11433–42

McLuckey SA, Glish GL, Van Berkel GJ. 1991a. Charge determination of product ions formed from collision-induced dissociation of multiply protonated molecules via ion/molecule reactions. *Anal. Chem.* 63(18):1971–78

McLuckey SA, Goeringer DE. 1995. Ion/Molecule Reactions for Improved Effective Mass Resolution in Electrospray Mass Spectrometry. *Anal. Chem.* 67(14):2493–97

McLuckey SA, Goeringer DE, Glish GL. 1991b. Selective ion isolation/rejection over a broad mass range in the quadrupole ion trap. *J. Am. Soc. Mass Spectrom.* 2(1):11–21

McLuckey SA, Huang T-Y. 2009. Ion/Ion Reactions: New Chemistry for Analytical MS. *Anal. Chem.* 81(21):8669–76

McLuckey SA, Stephenson JL. 1998. Ion/ion chemistry of high-mass multiply charged ions. *Mass Spectrom. Rev.* 17(6):369–407

McLuckey SA, Stephenson JL, Asano KG. 1998. Ion/Ion Proton-Transfer Kinetics: Implications for Analysis of Ions Derived from Electrospray of Protein Mixtures. *Anal. Chem.* 70(6):1198–1202

Ogorzalek Loo RR, Smith RD. 1994. Investigation of the Gas-Phase Structure of Electrosprayed Proteins Using Ion-Molecule Reactions. *J. Am. Soc. Mass Spectrom.* 5(4):207–20

Ogorzalek Loo RR, Udseth HR, Smith RD. 1992. A new approach for the study of gas-phase ion-ion reactions using electrospray ionization. *J. Am. Soc. Mass Spectrom.* 3(7):695–705

Pacholarz KJ, Barran PE. 2016. Use of a charge reducing agent to enable intact mass analysis of cysteine-linked antibody-drug-conjugates by native mass spectrometry. *EuPA Open Proteomics*. 11:23–27

Pepin R, Laszlo KJ, Marek A, Peng B, Bush MF, et al. 2016a. Toward a Rational Design of Highly Folded Peptide Cation Conformations. 3D Gas-Phase Ion Structures and Ion Mobility Characterization. *J. Am. Soc. Mass Spectrom.* 27(10):1647–60

Pepin R, Laszlo KJ, Peng B, Marek A, Bush MF, Tureček F. 2014. Comprehensive Analysis of Gly-Leu-Gly-Gly-Lys Peptide Dication Structures and Cation-Radical Dissociations Following Electron Transfer: From Electron Attachment to Backbone Cleavage, Ion–Molecule Complexes, and Fragment Separation. *J. Phys. Chem. A*. 118(1):308–24

Pepin R, Petrone A, Laszlo KJ, Bush MF, Li X, Tureček F. 2016b. Does Thermal Breathing Affect Collision Cross Sections of Gas-Phase Peptide Ions? An Ab Initio Molecular Dynamics Study. *J. Phys. Chem. Lett.* 7(14):2765–71

Pierson NA, Valentine SJ, Clemmer DE. 2010. Evidence for a Quasi-Equilibrium Distribution of States for Bradykinin $[M + 3H]^{3+}$ Ions in the Gas Phase. *J. Phys. Chem. B*. 114(23):7777–83

Pitteri SJ, Chrisman PA, Hogan JM, McLuckey SA. 2005. Electron Transfer Ion/Ion Reactions in a Three-Dimensional Quadrupole Ion Trap: Reactions of Doubly and Triply Protonated Peptides with $SO_2^{\bullet -}$. *Anal. Chem.* 77(6):1831–39

Pitteri SJ, McLuckey SA. 2005. Recent developments in the ion/ion chemistry of high-mass multiply charged ions. *Mass Spectrom. Rev.* 24(6):931–58

Putnam C. 2006. Protein Calculator

Rabuck JN, Hyung S-J, Ko KS, Fox CC, Soellner MB, Ruotolo BT. 2013. Activation State-Selective Kinase Inhibitor Assay Based on Ion Mobility-Mass Spectrometry. *Anal. Chem.* 85(15):6995–7002

1176 Riley NM, Westphall MS, Coon JJ. 2017. Activated Ion-Electron Transfer Dissociation Enables
1177 Comprehensive Top-Down Protein Fragmentation. *J. Proteome Res.* 16(7):2653–59
1178 Rolland AD, Biberic LS, Prell JS. 2022. Investigation of Charge-State-Dependent Compaction of
1179 Protein Ions with Native Ion Mobility–Mass Spectrometry and Theory. *J. Am. Soc. Mass*
1180 *Spectrom.* 33(2):369–81
1181 Salbo R, Bush MF, Naver H, Campuzano I, Robinson CV, et al. 2012. Traveling-wave ion
1182 mobility mass spectrometry of protein complexes: accurate calibrated collision cross-
1183 sections of human insulin oligomers: Traveling-wave IM-MS of protein complexes.
1184 *Rapid Commun. Mass Spectrom.* 26(10):1181–93
1185 Scalf M, Westphall MS, Smith LM. 2000. Charge Reduction Electrospray Mass Spectrometry.
1186 *Anal. Chem.* 72(1):52–60
1187 Schnier PD, Gross DS, Williams ER. 1995. Electrostatic Forces and Dielectric Polarizability of
1188 Multiply Protonated Gas-Phase Cytochrome c Ions Probed by Ion/Molecule Chemistry. *J.*
1189 *Am. Chem. Soc.* 117(25):6747–57
1190 Sever AIM, Konermann L. 2020. Gas Phase Protein Folding Triggered by Proton Stripping
1191 Generates Inside-Out Structures: A Molecular Dynamics Simulation Study. *J. Phys.*
1192 *Chem. B*. 124(18):3667–77
1193 Shelimov KB, Clemmer DE, Hudgins RR, Jarrold MF. 1997. Protein Structure *in Vacuo* : Gas-
1194 Phase Conformations of BPTI and Cytochrome *c*. *J. Am. Chem. Soc.* 119(9):2240–48
1195 Shelimov KB, Jarrold MF. 1997. Conformations, Unfolding, and Refolding of Apomyoglobin in
1196 Vacuum: An Activation Barrier for Gas-Phase Protein Folding. *J. Am. Chem. Soc.*
1197 119(13):2987–94

1198 Stephenson JL, McLuckey SA. 1996a. Ion/Ion Reactions in the Gas Phase: Proton Transfer
1199 Reactions Involving Multiply-Charged Proteins. *J. Am. Chem. Soc.* 118(31):7390–97
1200 Stephenson JL, McLuckey SA. 1996b. Ion/Ion Proton Transfer Reactions for Protein Mixture
1201 Analysis. *Anal. Chem.* 68(22):4026–32
1202 Stephenson JL, McLuckey SA. 1997. Adaptation of the Paul trap for study of the reaction of
1203 multiply charged cations with singly charged anions. *Int. J. Mass Spectrom. Ion Process.*
1204 162(1–3):89–106
1205 Stephenson JL, Van Berkel GJ, McLuckey SA. 1997. Ion-ion proton transfer reactions of bio-
1206 ions involving noncovalent interactions: Holomyoglobin. *J. Am. Soc. Mass Spectrom.*
1207 8(6):637–44
1208 Sterling HJ, Daly MP, Feld GK, Thoren KL, Kintzer AF, et al. 2010. Effects of supercharging
1209 reagents on noncovalent complex structure in electrospray ionization from aqueous
1210 solutions. *J. Am. Soc. Mass Spectrom.* 21(10):1762–74
1211 Sterling HJ, Prell JS, Cassou CA, Williams ER. 2011. Protein Conformation and Supercharging
1212 with DMSO from Aqueous Solution. *J. Am. Soc. Mass Spectrom.* 22(7):s13361-011-
1213 0116–x
1214 Sterner JL, Johnston MV, Nicol GR, Ridge DP. 1999. Apparent proton affinities of highly
1215 charged peptide ions. *J. Am. Soc. Mass Spectrom.* 10(6):483–91
1216 Syka JEP, Coon JJ, Schroeder MJ, Shabanowitz J, Hunt DF. 2004. Peptide and protein sequence
1217 analysis by electron transfer dissociation mass spectrometry. *Proc. Natl. Acad. Sci.*
1218 101(26):9528–33
1219 Syrstad EA, Turecček F. 2005. Toward a general mechanism of electron capture dissociation. *J.*
1220 *Am. Soc. Mass Spectrom.* 16(2):208–24

Tian Y, Han L, Buckner AC, Ruotolo BT. 2015. Collision Induced Unfolding of Intact Antibodies: Rapid Characterization of Disulfide Bonding Patterns, Glycosylation, and Structures. *Anal. Chem.* 87(22):11509–15

Townsend JA, Keener JE, Miller ZM, Prell JS, Marty MT. 2019. Imidazole Derivatives Improve Charge Reduction and Stabilization for Native Mass Spectrometry. *Anal. Chem.* 91(22):14765–72

Turecček F, Chen X, Hao C. 2008. Where Does the Electron Go? Electron Distribution and Reactivity of Peptide Cation Radicals Formed by Electron Transfer in the Gas phase. *J. Am. Chem. Soc.* 130(27):8818–33

Tureček F, Julian RR. 2013. Peptide Radicals and Cation Radicals in the Gas Phase. *Chem. Rev.* 113(8):6691–6733

Valentine SJ, Anderson JG, Ellington AD, Clemmer DE. 1997a. Disulfide-Intact and -Reduced Lysozyme in the Gas Phase: Conformations and Pathways of Folding and Unfolding. *J. Phys. Chem. B*. 101(19):3891–3900

Valentine SJ, Clemmer DE. 1997. H/D Exchange Levels of Shape-Resolved Cytochrome *c* Conformers in the Gas Phase. *J. Am. Chem. Soc.* 119(15):3558–66

Valentine SJ, Counterman AE, Clemmer DE. 1997b. Conformer-dependent proton-transfer reactions of ubiquitin ions. *J. Am. Soc. Mass Spectrom.* 8(9):954–61

Vidarsson G, Dekkers G, Rispens T. 2014. IgG Subclasses and Allotypes: From Structure to Effector Functions. *Front. Immunol.* 5:

Wang G, Cole RB. 1997. Solution, gas-phase, and instrumental parameter influences on charge-state distributions in electrospray ionization mass spectrometry. In *Electrospray*

Ionization Mass Spectrometry: Fundamentals, Instrumentation, and Applications, ed. RB Cole, pp. 137–74. New York: Wiley

Williams JP, Brown JM, Campuzano I, Sadler PJ. 2010. Identifying drug metallation sites on peptides using electron transfer dissociation (ETD), collision induced dissociation (CID) and ion mobility-mass spectrometry (IM-MS). *Chem. Commun.* 46(30):5458

Wyttenbach T, Bowers MT. 2011. Structural Stability from Solution to the Gas Phase: Native Solution Structure of Ubiquitin Survives Analysis in a Solvent-Free Ion Mobility–Mass Spectrometry Environment. *J. Phys. Chem. B*. 115(42):12266–75

Xia Y, Han H, McLuckey SA. 2008. Activation of Intact Electron-Transfer Products of Polypeptides and Proteins in Cation Transmission Mode Ion/Ion Reactions. *Anal. Chem.* 80(4):1111–17

Yang Y, Niu C, Bobst CE, Kaltashov IA. 2021. Charge Manipulation Using Solution and Gas-Phase Chemistry to Facilitate Analysis of Highly Heterogeneous Protein Complexes in Native Mass Spectrometry. *Anal. Chem.* 93(7):3337–42

Zhao Q, Soyk MW, Schieffer GM, Fuhrer K, Gonin MM, et al. 2009. An ion trap-ion mobility-time of flight mass spectrometer with three ion sources for ion/ion reactions. *J. Am. Soc. Mass Spectrom.* 20(8):1549–61

Zhong Y, Hyung S-J, Ruotolo BT. 2011. Characterizing the resolution and accuracy of a second-generation traveling-wave ion mobility separator for biomolecular ions. *The Analyst*. 136(17):3534

Zubarev RA, Kelleher NL, McLafferty FW. 1998. Electron Capture Dissociation of Multiply Charged Protein Cations. A Nonergodic Process. *J. Am. Chem. Soc.* 120(13):3265–66

Biographies

Associate Professor Matthew F. Bush pursued his PhD with Evan Williams and Richard Saykally at the University of California, Berkeley. During that time, he used infrared laser spectroscopy and Fourier-transform mass spectrometry (MS) to investigate zwitterion formation and ion solvation. This training in high-performance MS and physical chemistry laid the groundwork for his continued pursuits using gas-phase techniques to investigate the structures and interactions of biomolecules. He then joined the laboratory of Carol Robinson FRS DBE at the University of Cambridge and the University of Oxford, during which time he used ion mobility MS to characterize the structures of biomolecules, large and small. He joined the chemistry faculty at the University of Washington in 2011. His research group develops MS-based approaches for elucidating the structures, interactions, and dynamics of biomolecules. They apply those approaches to a wide range of biological systems, with a focus on those involved in homeostasis.

Theresa Gozzo obtained her bachelor's degree in chemistry from The College of William and Mary under the advisement of Dr. John C. Poutsma. After her introduction to proteomic research, she moved to Seattle to specialize in ion mobility-mass spectrometry of intact proteins in the Bush lab at the University of Washington. She is currently a PhD candidate and will complete her degree in analytical chemistry in 2023. Her research focuses on probing the effects of charge on gas-phase ion structures and increasing the information content of ion mobility experiments.

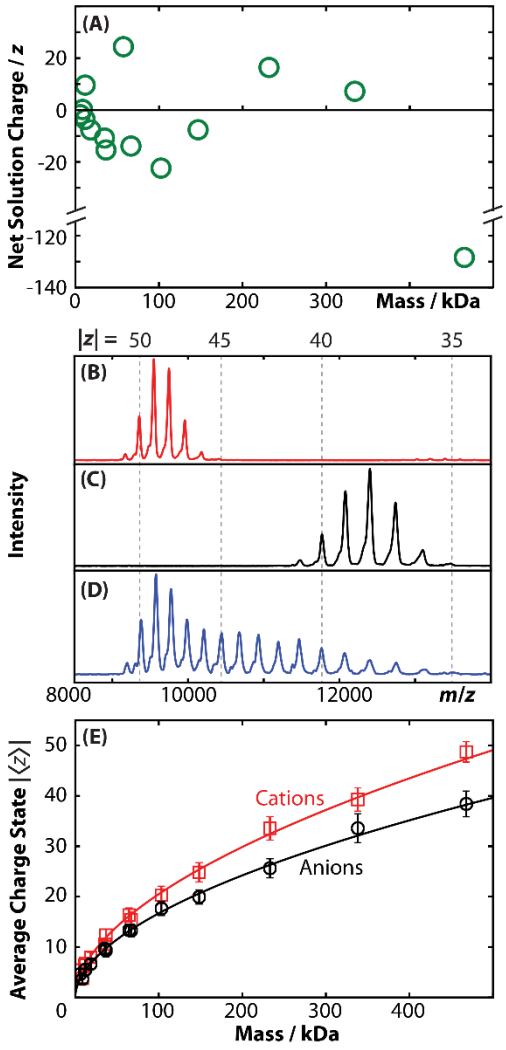

1289

1290 **Figure 1.** (A) Net charges of proteins in solution estimated based on the pK_a of constituent
1291 amino acids (Putnam 2006). NanoESI of β-galactosidase in 200 mM ammonium acetate at pH
1292 7.0 measured in (B) positive and (C) negative polarities. Spectrum D is similar to spectrum B,
1293 but the solution also contained 10 mM triethylamine and additional charge-reduced cations were
1294 also observed. (E) Absolute value of the average charge states of selected protein and protein
1295 complex ions in positive (*red*) and negative (*black*) ion mode as a function of mass. Power
1296 functions are fit to the data to serve as a guide to the eye. The bars on those markers span two
1297 standard deviations of the observed charge-state distribution. The mean and width of each
1298 charge-state distribution varied little between experiments performed over several months.
1299 Figure and caption adapted with permission from (Allen et al. 2013).

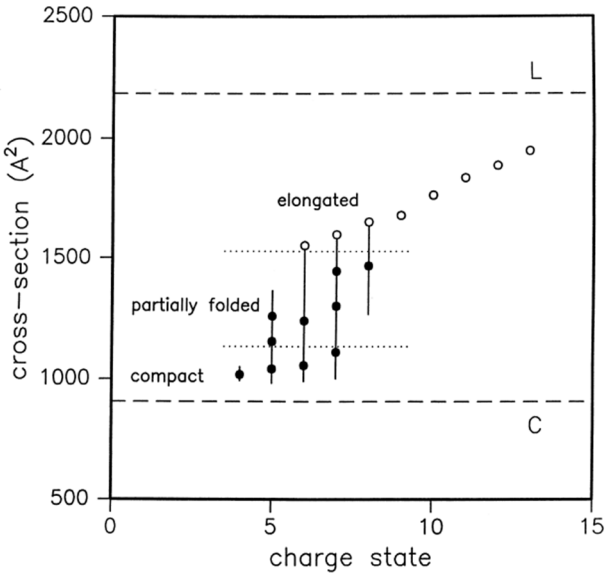

Figure 2. Experimental collision cross sections for all conformations and charge states observed for ubiquitin, including those produced via charge reduction. 6+ to 13+ charge states were observed directly from ESI from 1:1 water: acetonitrile with 2% acetic acid. The vertical lines correspond to a distribution of unresolved conformations having a range of collision cross sections. The filled circles that are superimposed on the lines correspond to reproducible maxima in the unresolved spectra. The horizontal dashed lines correspond to the calculated cross sections for the crystal conformer (C) and the near-linear conformer (L). Horizontal dotted lines are used to divide the data into three conformer types: compact, partially folded, and elongated. Figure and caption adapted with permission from (Valentine et al. 1997b).

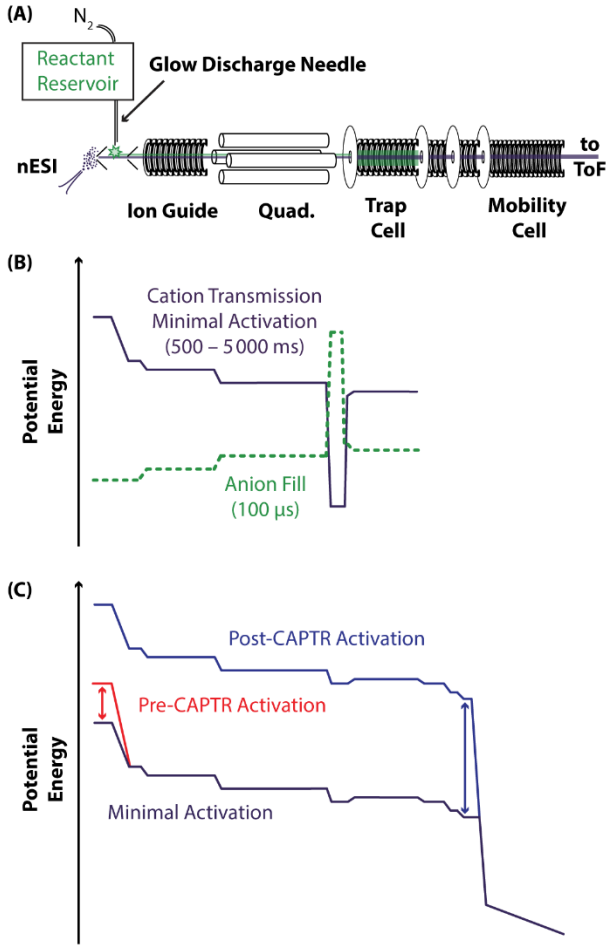

Figure 3. (A) Diagram of the modified Waters Synapt G2 HDMS used in these experiments. Anions (green) are generated by glow-discharge ionization and accumulated in the trap cell. Cations (purple) are generated by nanoESI and are trapped with anions for CAPTR. Residual precursor and CAPTR product ions are separated using IM in a radio-frequency confining drift cell prior to mass analysis. (B) Relative potentials applied to selected ion optics during cation transmission (*solid purple line*) and anion fill (*dashed green line*). (C) Representative potential-energy diagrams for cation transmission during minimal activation, pre-CAPTR activation, and post-CAPTR activation experiments. Panels (A) and (C) and associated caption adapted with permission from (Laszlo et al. 2016). Panel (B) and associated caption adapted with permission from (Laszlo & Bush 2015).

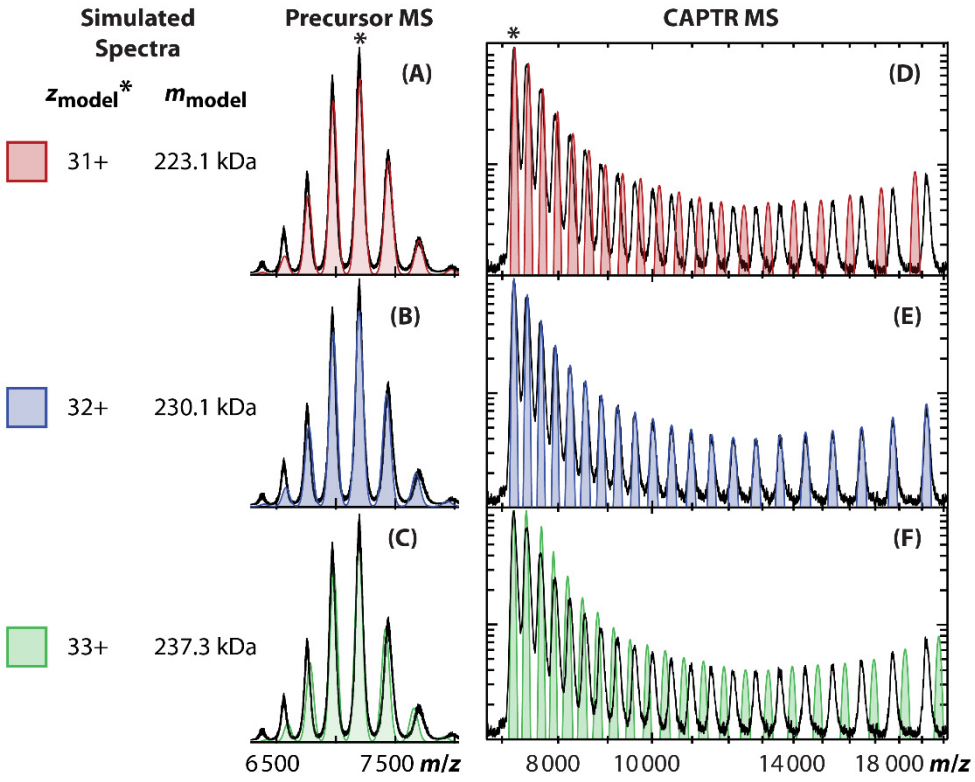

Figure 4. (A) to (C) each show a simulated spectrum (*blue, red, and green)* modeling the experimental native mass spectrum of pyruvate kinase (*black*). Assigning the base peak at *m*/*z* 7200 a charge of 31+ (A, *red*), 32+ (B, *blue*), or 33+ (C, *green*) results in apparent masses of 223.1, 230.3, and 237.3 kDa, respectively; (D) to (F) each show a simulated spectrum modeling the experimental CAPTR spectrum for the *m*/*z* 7200 peak of pyruvate kinase. These spectra were simulated using the mass determined for the corresponding model of the native mass spectrum. Intensities were set manually to resemble the intensities in the experimental spectrum. Figure and caption adapted with permission from (Laszlo & Bush 2015).

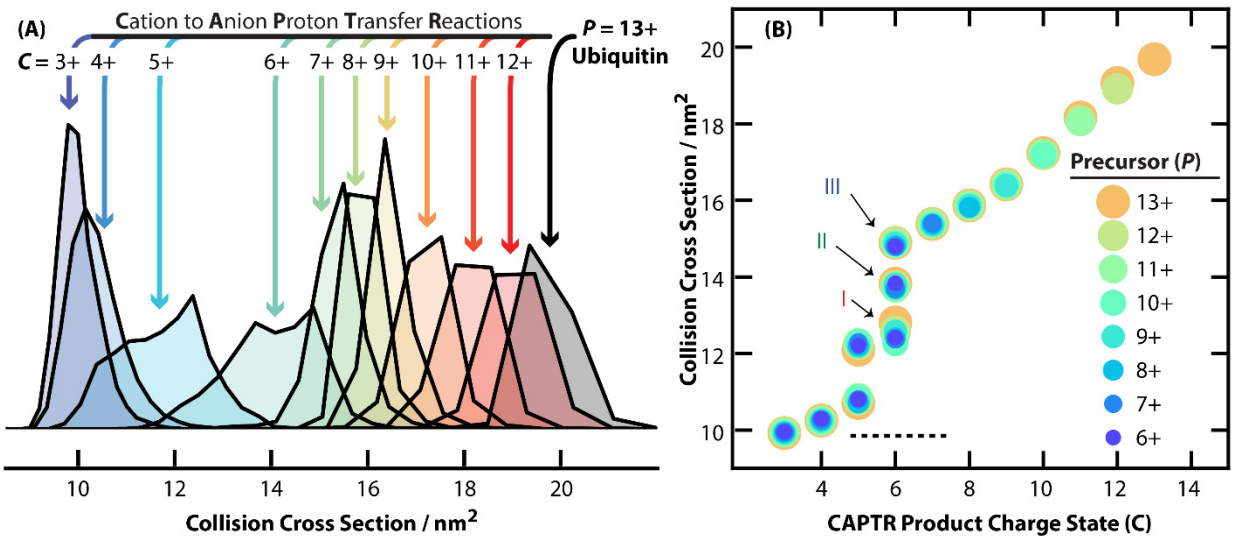

1331

1332 **Figure 5.** (A) Normalized Ω distributions of all 13→*C* ions of ubiquitin. All ions except 13→6

1333 and 13→5 exhibit monomodal Ω distributions. 13→6 and 13→5 exhibit trimodal and bimodal Ω

1334 distributions, respectively. (B) Ω of precursor (*P*) and CAPTR product ions (*P*→*C*) of ubiquitin.

1335 The lowest charge state product detected for each precursor ion was 3+. Precursor charge states

1336 are represented by differently colored circles, which were selected to facilitate visualization of

1337 the data. Average Ω of 4+ to 6+ ubiquitin from a native-like solution (Salbo et al. 2012) is shown

1338 with a dotted line for comparison. Figure and caption adapted with permission from (Laszlo et al.

1339 2016).

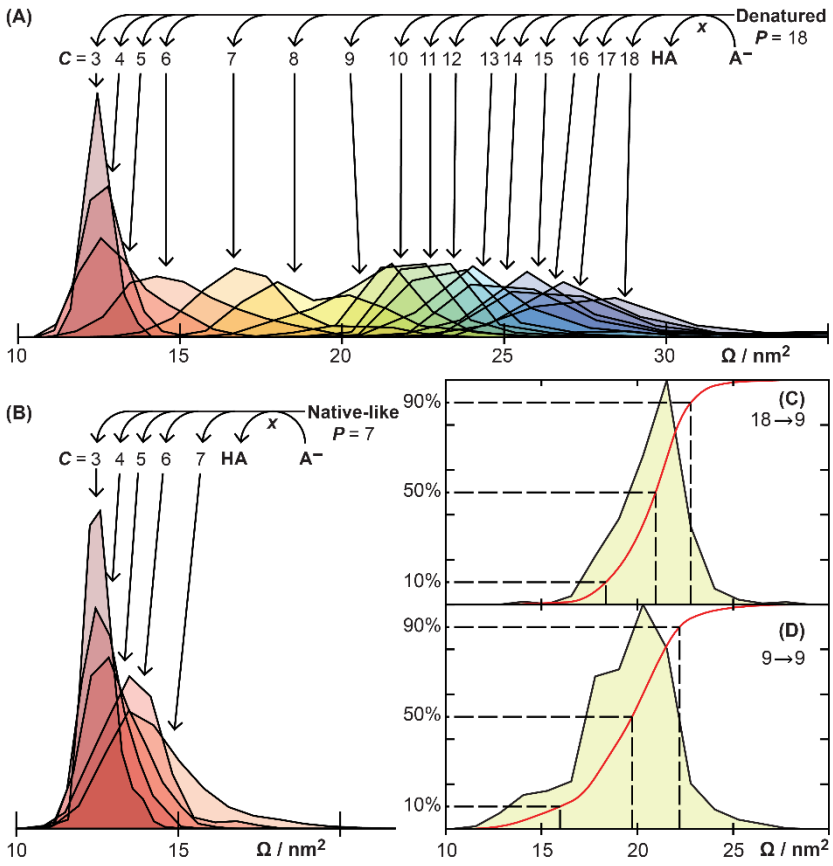

1340

1341 **Figure 6.** (A) Apparent Ω distributions for all 18→*C* ions of cytochrome *c* from denaturing

1342 conditions. (B) Ω distributions for all 7→*C* ions of cytochrome *c* from native-like conditions.

1343 The Ω distribution (*black solid lines*), cumulative distribution (*red lines*), and critical Ω values

1344 (*black dashed lines*) for the (C) 18→9 and (D) 9→9 ions from denaturing conditions. All

1345 experiments probed ions generated using a temperature-controlled, ESI source set to 25 °C.

1346 Figure and caption adapted with permission from (Laszlo et al. 2017a).

1347

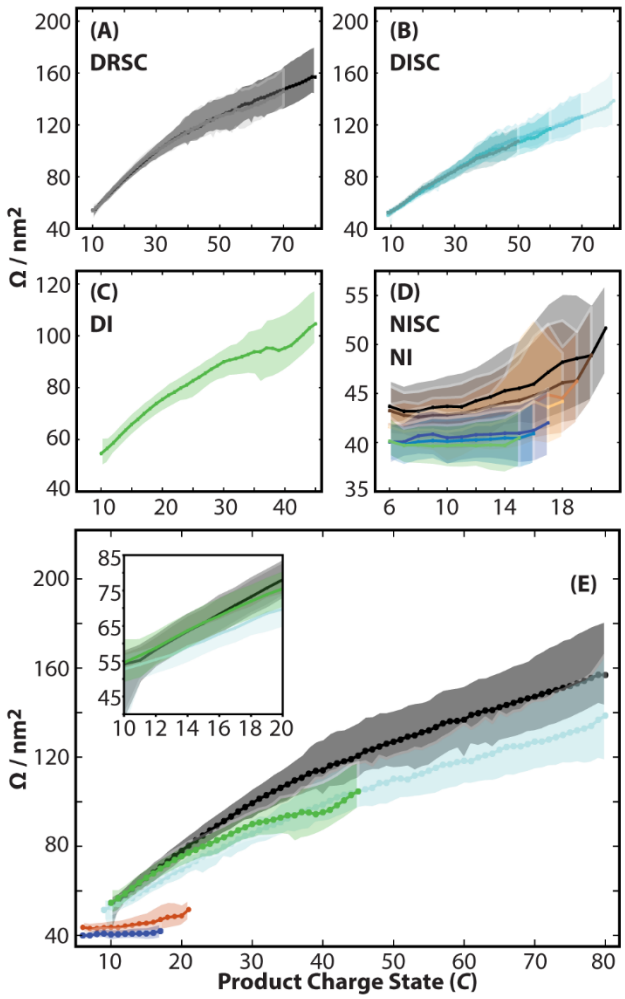

Figure 7. Results from IM-MS of CAPTR products of bovine serum albumin ions generated from various solution conditions. Markers correspond to the $\tilde{\Omega}$ (median) values and the shaded regions span from 10% to 90% of the cumulative distribution function of each apparent Ω distribution. Results for (A) the $^{DRSC}P \rightarrow C$, P = 70 and 80, ions, (B) the $^{DISC}P \rightarrow C$, P = 50, 60, 70, and 80, ions, (C) the $^{DI}45 \rightarrow C$ ions, and (D) the $^{NISC}P \rightarrow C$, P = 18 to 21 (*copper tones*), and the $^{NI}P \rightarrow C$, P = 15 to 17 (*cool tones*), ions. (E) Summary of results for the highest P from each solution condition, *i.e.*, the $^{DRSC}80 \rightarrow C$, $^{DISC}80 \rightarrow C$, $^{DI}45 \rightarrow C$, $^{NISC}21 \rightarrow C$, and $^{NI}17 \rightarrow C$ ions. The inset of E shows the results for $^{DRSC}80 \rightarrow C$, $^{DISC}80 \rightarrow C$, $^{DI}45 \rightarrow C$ ions for $20 \geq C \geq 10$. Figure and caption adapted with permission from (Gadzuk-Shea & Bush 2018).

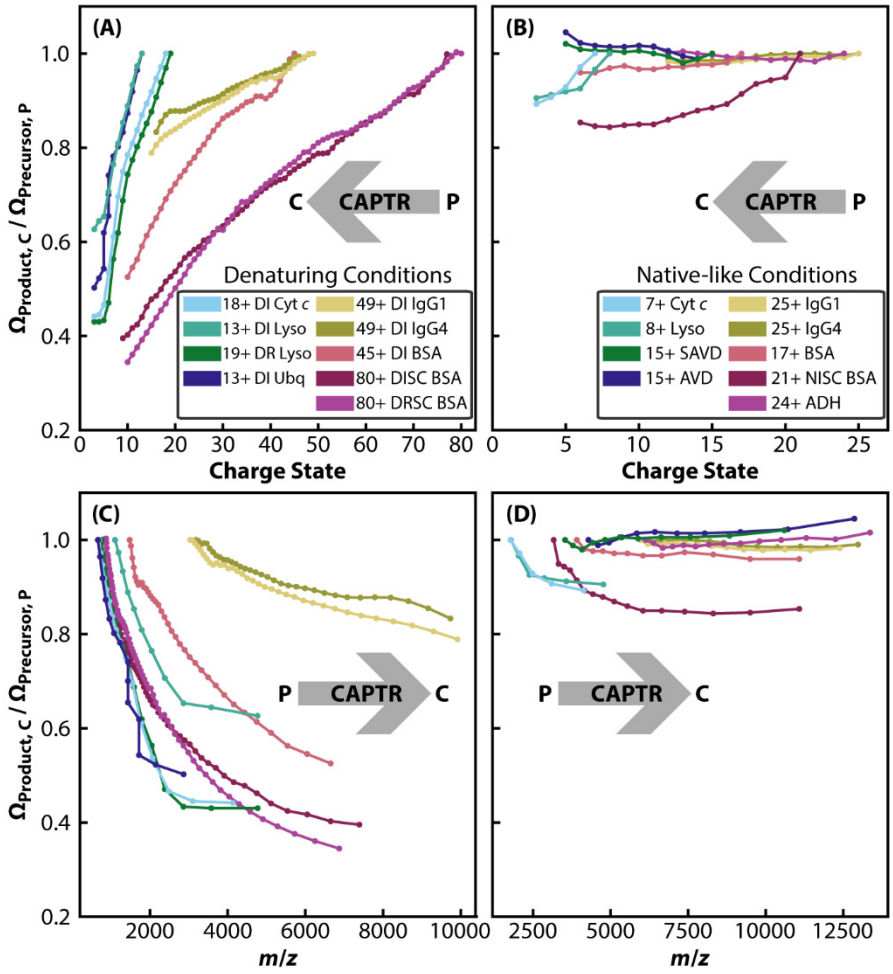

1358

1359 **Figure 8.** Summary of CAPTR results across different studies. **Ω** values used to determine
1360 $\Omega_{Product}/\Omega_{Precursor}$ correspond to either the centroid values of the Gaussian fits of the **Ω**
1361 distributions or to the 50% critical value calculated from cumulative distributions functions
1362 (integrations of apparent **Ω** distributions), depending on the study. Panels (A) and (C) show
1363 results from protein ions generated by ESI from native-like conditions. Panels (B) and (D) show
1364 results from protein ions generated from denaturing conditions. Panels (A) and (B) represent
1365 $\Omega_{Product}/\Omega_{Precursor}$ as a function of charge state, so precursors are of the highest charge and have
1366 $\Omega_{Product}/\Omega_{Precursor}$ equal to 1.0. Panels (C) and (D) represent $\Omega_{Product}/\Omega_{Precursor}$ as a function of *m*/*z*,
1367 so precursors are of the lowest *m*/*z*. Protein abbreviations are as follows: cytochrome *c* (cyt *c*),
1368 lysozyme (lyso), ubiquitin (ubq), bovine serum albumin (BSA), streptavidin (SAVD), avidin
1369 (AVD), and alcohol dehydrogenase (ADH).

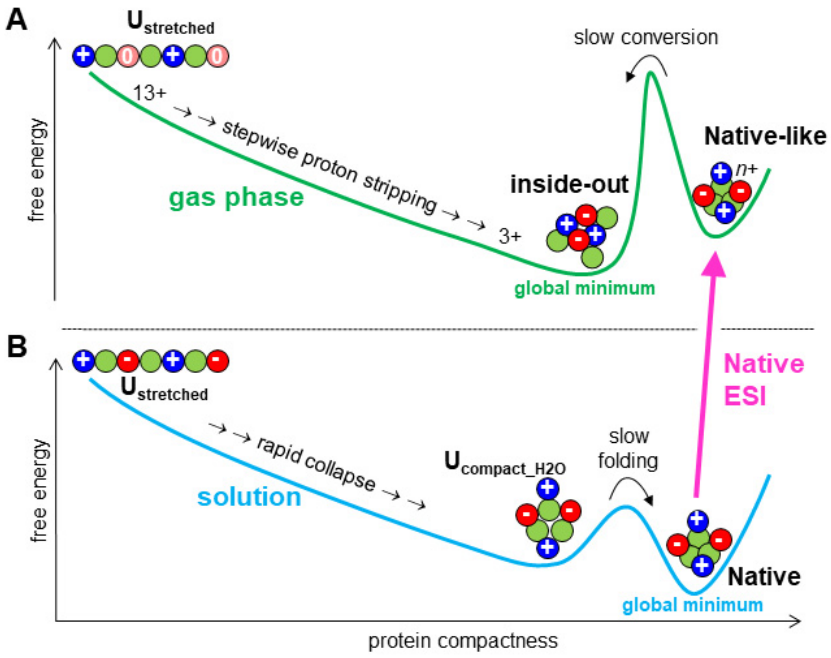

1370

1371 **Figure 9**. Cartoon summary of protein folding (A) in the gas phase and (B) in aqueous solution.

1372 Native ESI provides a connection between the two energy landscapes. Protein chains are shown

1373 in hydrophobic (green) and hydrophilic (positive/blue, negative/red) residues. An extended

1374 $U_{stretched}$ conformation was included in part B to facilitate comparisons with the gas-phase

1375 behavior; we do not suggest that folding in solution generally starts from $U_{stretched}$. Figure and

1376 caption adapted with permission from (Sever & Konermann 2020).

1377

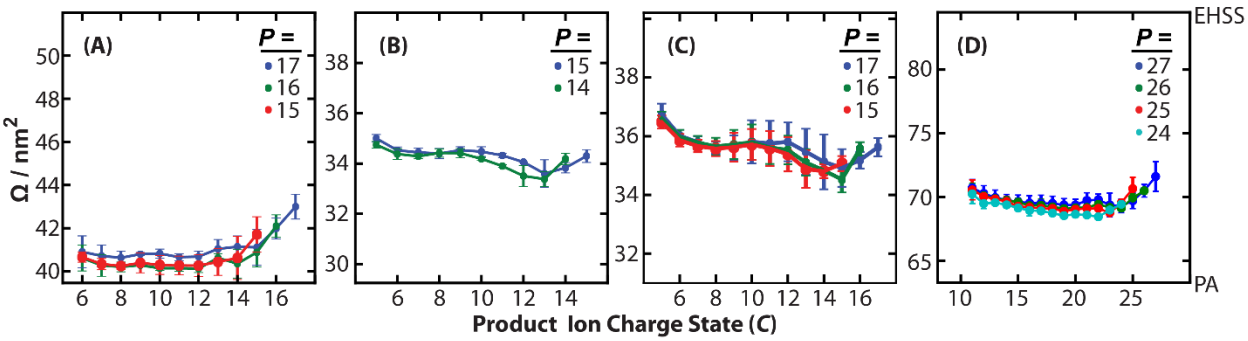

1378

1379 **Figure 10.** Ω values of the *P*→*C* ions of (A) serum albumin, (B) streptavidin, (C) avidin and (D)

1380 alcohol dehydrogenase, where "*P*" is the charge state of the precursor and "*C*" is the charge state

1381 of the CAPTR product. The bars span the 95% confidence interval for each value, and the upper

1382 and lower limits of each panel correspond to the Ω values calculated using the projection

1383 approximation, PA, and exact hard spheres scattering, EHSS, methods. The different colors

1384 indicate ions from different *P*. Figure and caption adapted with permission from (Laszlo & Bush

1385 2017).

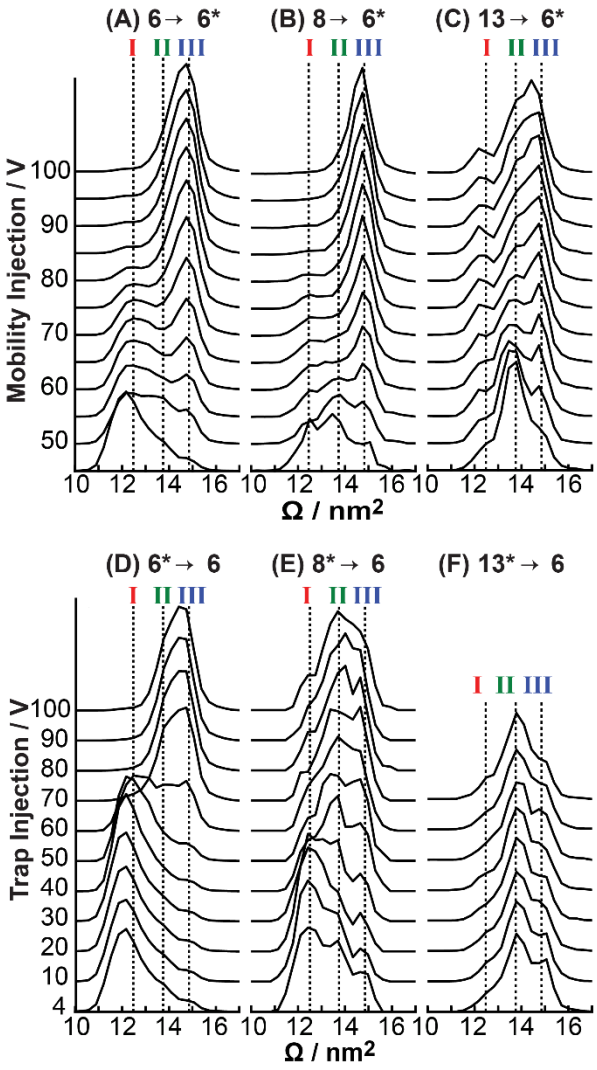

1386

1387 **Figure 11.** Post-CAPTR activation of (A) 6→6*, (B) 8→6*, and (C) 13→6* ubiquitin ions. Pre-

1388 CAPTR activation of (D) 6*→6, (E) 8*→6, and (F) 13*→6 ubiquitin ions. Vertical lines

1389 corresponding to the average Ω for the three features of the Ω distribution of 6+ (I to III) from

1390 Figure 5B are included for comparison. These mobility experiments used a field of 6.4 $V \cdot cm^{-1}$.

1391 Figure and caption adapted with permission from (Laszlo et al. 2016).

1392

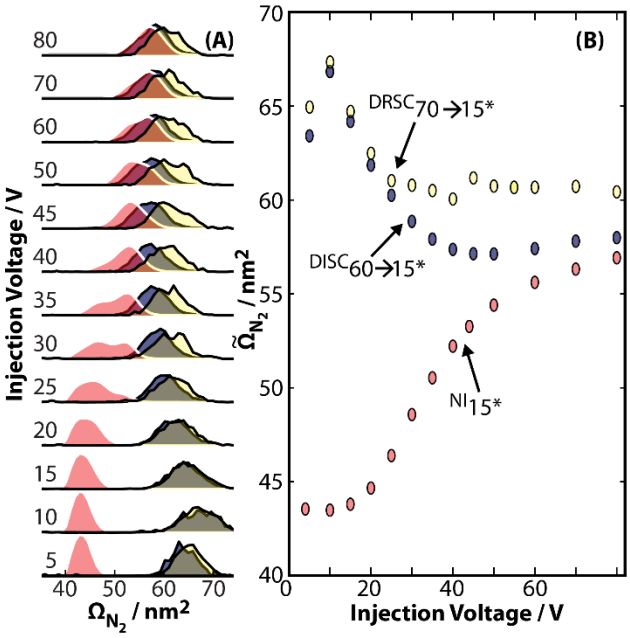

1393

1394 **Figure 12.** (A) Apparent Ω_{N_2} distributions of the ^{NI}15* (*magenta*), ^{DISC}60→15* (*purple*), and

1395 ^{DISC}70→15* (*yellow*) BSA ions as a function of the injection voltage used to transfer the ions

1396 into a drift cell containing 1.2 Torr nitrogen gas. (B) $\tilde{\Omega}_{N_2}$ values of the distributions in panel A as

1397 a function of the injection voltage. Figure and caption adapted with permission from (Gadzuk-

1398 Shea & Bush 2018).

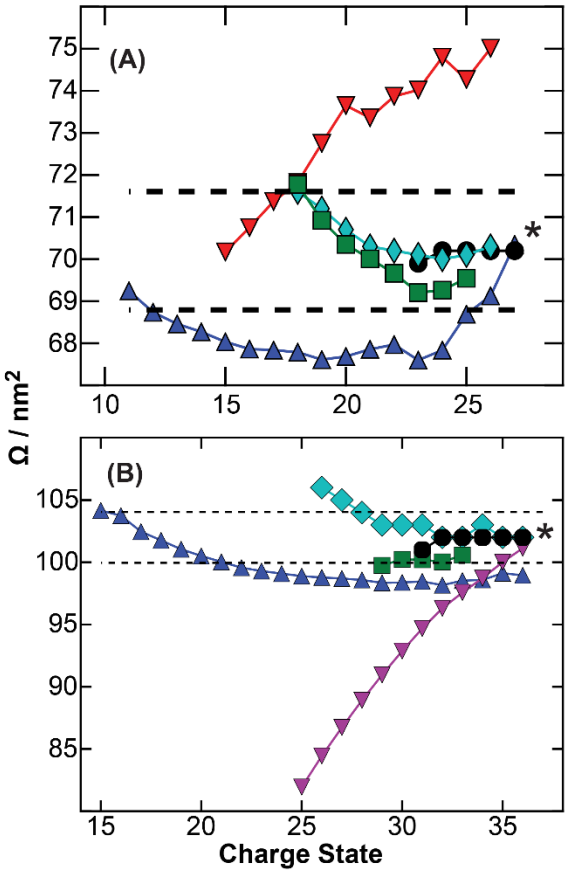

Figure 13. Ω values for (A) alcohol dehydrogenase and (B) pyruvate kinase ions. Results from CAPTR (*blue triangles*) are based on the average of the values for the products from each precursor (Laszlo & Bush 2017). For comparison, values are also plotted for ions generated from ESI of solutions containing 200 mM ammonium acetate at pH 7.0, *black circles*, (Allen et al. 2013), 200 mM ammonium acetate with 10 mM triethylamine at pH 7.0, *cyan diamonds*, (Allen et al. 2013), 100 mM ammonium acetate at pH 6.9 with exposure to nebulized 1,5-diazabicyclo[4,3,0]non-5-ene, DBU, *green squares* (Bornschein et al. 2011), 100 mM ammonium acetate at pH 6.9 and reacted with 1,4-dicyanobenzene radical anions, *red inverted triangles*, (Lermyte et al. 2015), and 100 mM ammonium acetate in close proximity to a corona discharge probe, *purple inverted* triangles, (Campuzano & Schnier 2013). Dashed horizontal lines indicate ±2% of the data point marked with an asterisk (*). Figure and caption adapted with permission from (Laszlo & Bush 2017).

1413

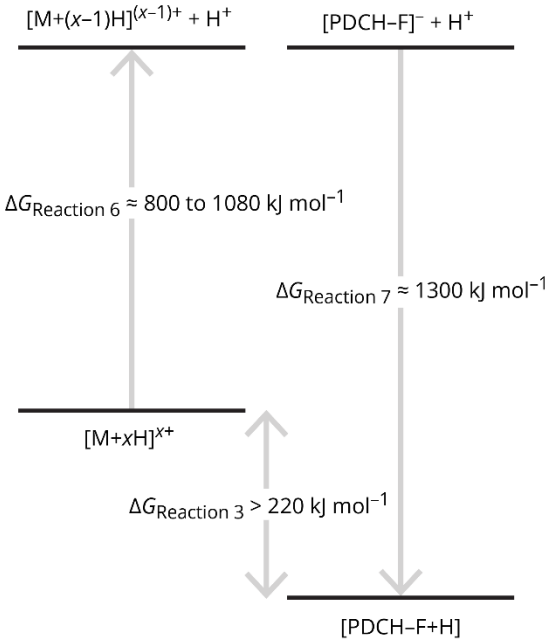

1414

1415 **Figure 14.** Partial reactions that were used to estimate the exergonicty of each CAPTR event

1416 (Reaction 3). See text for a discussion of these estimates.